Univerzita Karlova

Přírodovědecká fakulta

Studijní program: Makromolekulární chemie

Navazující magisterský studijní odbor: Makromolekulární chemie

Bc. Soňa Mesíková

Nanomateriály založené na interakcích nanoiontů s hydrofilními polymery

Nanomaterials based on nano-ion hydrophylic polymer interactions

Diplomová práce

Školitel: doc. RNDr. Pavel Matějíček, Ph.D.

Konzultant: Ing. Mariusz Uchman, Ph.D.

Praha, 2022

Prohlášení:

Prohlašuji, že jsem závěrečnou práci zpracovala samostatně a že jsem uvedla všechny použité informační zdroje a literaturu. Tato práce ani její podstatná část nebyla předložena k získání jiného nebo stejného akademického titulu.

V Praze dne, 16.05.2022

Podpis

I would like to thank to my supervisor doc. RNDr. Pavel Matějíček, Ph.D., to my advisor Ing. Mariusz Uchman, Ph.D., and to prof. RNDr. Miroslav Štěpánek, Ph.D. for welcoming me to the Soft Matter group since the beginning of my studies at Charles University. Their advice and guidance always motivated me and encouraged me to pursue my research. I would also like to thank to my colleagues for their continuous help and permanently good mood in our laboratory. Especially I want to thank to M. Sc. Jianwei Li, PhD., for his patience, advice, and practical lesson. Special thanks go to my parents for providing me support throughout my years of study.

I would like to acknowledge the financial support of GAČR grant No. 19-13458S.

Abstrakt

Diplomová práce se zabývá asociačním chováním trojblokových kopolymerů poly(2-(N, N, N′, N′-tetramethyl guanidin)ethyl akrylát)-*b*-poly(ethylen oxid)-*b*-poly(2-(N, N, N′, N′-tetramethyl guanidin)ethyl akrylát), PGEA-PEO-PGEA, a poly(N-isopropylakrylamid)-*b*-poly(akrylová kyselina)-*b*-poly(N-isopropylakrylamid), PNIPAM-PAA-PNIPAM v přítomnosti aniontových klastrových sloučenin bóru *closo*-dodekaborátového aniontu, $[B_{12}H_{12}]^{2-}$ a [kobalt(3+) bis(1,2-dikarbollidového)] aniontu, COSAN, a dále pak vlivem solí na vznik komplexu homopolymeru poly(ethylen oxidu), PEO, s aniontem COSAN. V rámci práce byla provedena syntéza trojblokového kopolymeru PNIPAM-PAA-PNIPAM, byl studován vznik hydrogelů na základě interakcí kationtových bloků PGEA kopolymeru PGEA-PEO-PGEA s *closo*-dodekaborátovýn aniontem a na základě dvouvodíkové vazby neutrálních bloků PNIPAM kopolymeru PNIPAM-PAA-PNIPAM s aniontem COSAN. Mechanické vlastnosti gelů a jejich vnitřní struktura byly studovány pomocí technik reologie a pomocí rozptylových a fluorescenčních metod. Také byl studován vliv lithných a sodných solí na stabilitu komplexu PEO/COSAN ve vodných roztocích.

Abstract

The Thesis deals with the co-assembly of triblock copolymers poly(2-(N, N, N′, N′-tetramethyl guanidinium)ethyl acrylate)-*b*-poly(ethylene oxide)-*b*-poly(2-(N, N, N′, N′-tetramethyl guanidinium)ethyl acrylate), PGEA-PEO-PGEA, and poly(N-isopropylacrylamide)-*b*-poly(acrylic acid)-*b*-poly(N-isopropylacrylamide), PNIPAM-PAA-PNIPAM, with anionic boron cluster compounds *closo*-dodecaborate anion, $[B_{12}H_{12}]^{2-}$, and [cobalt(3+) bis(1,2-dicarbollide)] anion, COSAN, in aqueous solutions, respectively. Synthesis of PNIPAM-PAA-PNIPAM triblock copolymers was performed. The formation of gels based on electrostatic interactions of cationic blocks of PGEA-PEO-PGEA copolymer with *closo*-dodecaborate anion and on dihydrogen bonding of neutral PNIPAM blocks of PNIPAM-PEO-PNIPAM with COSAN was investigated. The inner structure of the gels was investigated by scattering techniques and fluorescent spectroscopy. Their mechanical properties were studied by diverse rheology measurements. Influence of lithium and sodium salts on PEO/COSAN complex formation and stability in aqueous solution was also studied.

Abbreviations

ABCC - anionic boron cluster compound

AIBN - 2,2′-Azobis(2-methylpropionitrile)

ATRP - atom transfer radical polymerization

BNCT - boron neutron capture therapy

CONTIN - constrained inverse Laplace transform routine

COSAN - [3-cobalt(3+) bis(1,2-dicarbolide)](1-); CObalt SANdwich

CTA - chain-transfer agents

DCM - dichlormethane

DHBC - double hydrophilic block copolymers

DLS - dynamic light scattering

DMA - N,N-dimethylacetamide

FBC - fluorescein-dodecaborane anion conjugate

HIV - human immunodeficiency virus

LCST - lower critical solution temperature

MeOH- methanol

NMR - nuclear magnetic resonance

PAA - poly(acrylic acid)

PEO - poly(ethylene oxide)

PGEA - poly(2-(N, N, N′, N′-tetramethyl guanidinium) ethyl acrylate)

PNIPAM - poly(N-isopropylacrylamide)

PMMA - poly(methyl methacrylate)

PtBA - poly(tert-butyl acrylate)

PTFE - poly(tetrafluorethylen)

RAFT- reversible addition-fragmentation chain-transfer polymerization

SAXS - small-angle X-ray scattering

SEC - size exclusion chromatography

SLS - static light scattering

TFA - trifluoroactetic acid

UCST - upper critical solution temperature

WAXS - wide-angle X-ray scattering

Content

1. Introduction

Multiblock copolymers are versatile building blocks for preparation of variety of nanostructures including micelles, nanogels or hydrogels in aqueous solutions. Architecture of block copolymers can utilize special properties like ion selectivity, thermoresponsivity or pH responsivity into one macromolecule. By introducing atypical ions such as anionic boron cluster compound, we can induce co-assembly of block copolymers into diverse nanoparticles, nanostructures and gels driven by electrostatic or weak interactions. These nanomaterials have possible applications in drug-delivery, boron neutron capture therapy, nanoelectronics, etc.

In this Thesis, the co-assembly of triblock copolymers of the A-B-A type with anionic boron cluster compounds was investigated. Poly(2-(N, N, N′, N′-tetramethyl guanidinium)ethyl acrylate)-*b*-poly(ethylene oxide)-*b*-poly(2-(N, N, N′, N′-tetramethyl guanidinium)ethyl acrylate), PGEA-PEO-PGEA, and poly(N-isopropylacrylamide)-*b*-poly(acrylic acid)-*b*-poly(N-isopropylacrylamide), PNIPAM-PAA-PNIPAM, triblock copolymers in aqueous solutions were used for the formation of hydrogels after mixing with sodium *closo*-dodecaborate, $Na_2[B_{12}H_{12}]$, or sodium cobalt bis(dicarbollide), Na[COSAN], respectively. Polymerization of triblock copolymers were tracked by NMR spectroscopy and SEC. The properties of the gels were studied by different scattering techniques, fluorescence spectroscopy and rheology. We also studied the formation of PEO/COSAN complexes in aqueous solution in the presence of the variety of lithium and sodium salts

The projects, which are included to this Thesis, were carried out in the frame of Soft Matter research team. All the studies would not be possible without cooperation with other team members and other colleges: PGEA-PEO-PGEA triblock copolymers were synthesized with help of M. Sc. Jianwei Li, PhD., fluorescence measurements were performed with help of Mgr. J. Sýkora, Ph.D. (Heyrovský Institute of Physical Chemistry in Prague), rheological measurements were performed at TU Berlin in the laboratory of Prof. Michael Gradzielski, and X-ray scattering data were provided by Ing. Jiří Brus, Dr. (Institute of Macromolecular Chemistry in Prague).

2. Overview of the literature

2.1. Reversible addition-fragmentation chain-transfer polymerization

Reversible addition-fragmentation chain-transfer polymerization (RAFT) is a type of controlled radical polymerization that gained a lot of attention in recent years. The main advantage of this method is the control over molecular weight distribution to achieve narrow polymer dispersity. Additionally, this method gives control over copolymer composition and polymer architecture.[0] Chain-transfer agents (CTA) also provide control over end-group functionalization. Generally, a RAFT-agent is compound with good radical leaving group and reactive double bond that can interact with propagating radical, which creates stable radical intermediate.[1, 2] Mechanism of RAFT polymerization (Figure 1) has many similarities to radical polymerization in the initiation, propagation and termination of polymer chains. The main difference is the chain transfer that is a key step in RAFT. In this step, the initiating radical reacts with monomer and provides propagating radical that interacts with the double of the CTA to create intermediate radical.[2, 3]

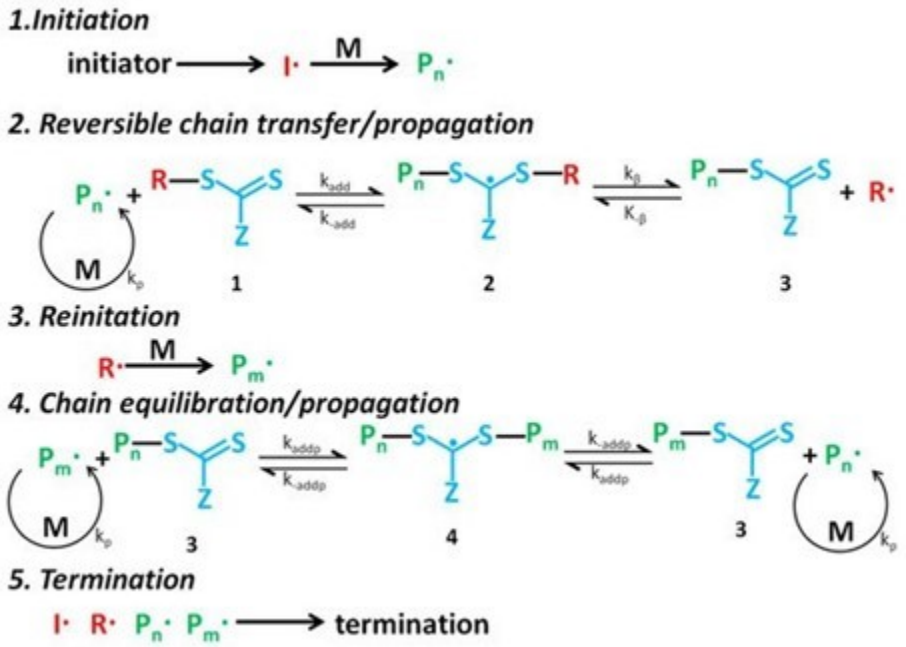

Figure 1: Mechanism of RAFT polymerization; scheme taken from Ref. 3.

Even though RAFT is relatively simple and can be used for wide range of monomers, a CTA that is well suited for specific monomer needs to be selected. For more activated monomers like styrenes and acrylates, dithiobenzoates can be used. For less activated monomers like

vinyl esters or vinyl amides, xantanes or dithiocarbamates can be used. From the CTAs, trithiocarbonates are considered universal and can be also synthesized with various functional groups.[3, 4, 5]

2.2. Anionic boron cluster compounds

Charged boranes, carboranes, metallacarboranes belong to the group called anionic boron cluster compounds (ABCCs) that are considered to be non-classical amphiphiles (Figure 2). They have an atypical shape due to the two-electron three-center bond, with delocalized electrons over the cluster that causes their three-dimensional aromaticity. Interactions of these clusters are influenced by electronegativity of the boron which is lower than the one of hydrogen and carbon. Boron clusters can form not only classical hydrogen bond but also dihydrogen bonds.[6,7]

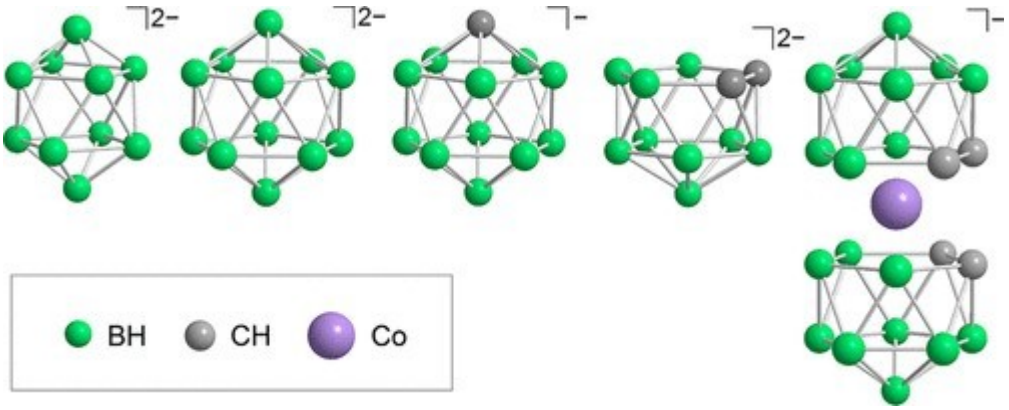

Figure 2: Structures of the most studied and common ABCCs (left to right): decaborate, dodecaborate, carbadodecaborate, 1,2-dicarbollide, COSAN; schematic structures taken from ref. 7.

Closo-dodecaborate is very stable compound that can withstand temperatures up to 800 °C and it is considered to be the most stable out of the ABCCs. Thanks to its high boron contend it is suitable for drug delivery and boron neutron capture therapy (BNCT). BNCT is based on reaction that follows the irradiation of boron isotope ^{10}B with neutrons. Over the years many dodecaborate derivates have been synthesized, because of the relatively easy functionalization of boron atoms in cluster.[7, 8, 9]

From the group of metallacarboranes a [3-cobalt bis(1,2-dicarbolide)] (COSAN) has gained a lot of attention thanks to its thermal and chemical stability. This cluster compound possesses typical properties of carboranes. The hydridic hydrogens on the surface of the COSAN cluster enables the creation of specific dihydrogen bonds. However, C-H units can be involved in classical hydrogen bonding. Even though the cluster has amphiphilic

characters, its salts are water-soluble.[7, 9] In recent years more and more papers study the interactions of COSAN with peptides or polymers and its complex synthetic possibilities. Poly(ethylene oxide) (PEO) is a versatile polymer when it comes to its biomedical applications. The PEO and COSAN form water insoluble complexes of plastic appearance and deep red colour. For preparation of stable polymeric nanoparticles containing COSAN, an optimization of conditions in the aqueous solution is very important. Not only the salt concentration is crucial to the stability of the complex but also chemical composition of the salt. System containing COSAN have a great potential when it comes to biomedical applications as inhibitor of HIV protease and in BNCT.[7, 9]

2.3. Stimuli responsive polymers

Stimuli responsive materials, also called "smart" materials, respond to changes in external stimuli for example pH, temperature, light, electrical or magnetic fields and others. Response to stimuli triggers change in properties of the material and can influence the collective behaviour of it. These materials have many possible applications, like in on-demand drug delivery, tissue engineering or biosensors.[10-12]

2.3.1. Thermoresponsive polymers

The ability of the material to respond to environmental temperature by changing its solubility is called thermoresponsivity. Thermoresponsive polymers are more and more studied and used in biomedical field, in drug delivery or tissue engineering since temperature is a stimulus that is easy to control. The two main types of thermoresponsive polymers are: i) polymers with upper critical solution temperature (UCST) and ii) polymers with lower critical solution temperature (LCST) (Figure 3).[10, 11, 12]

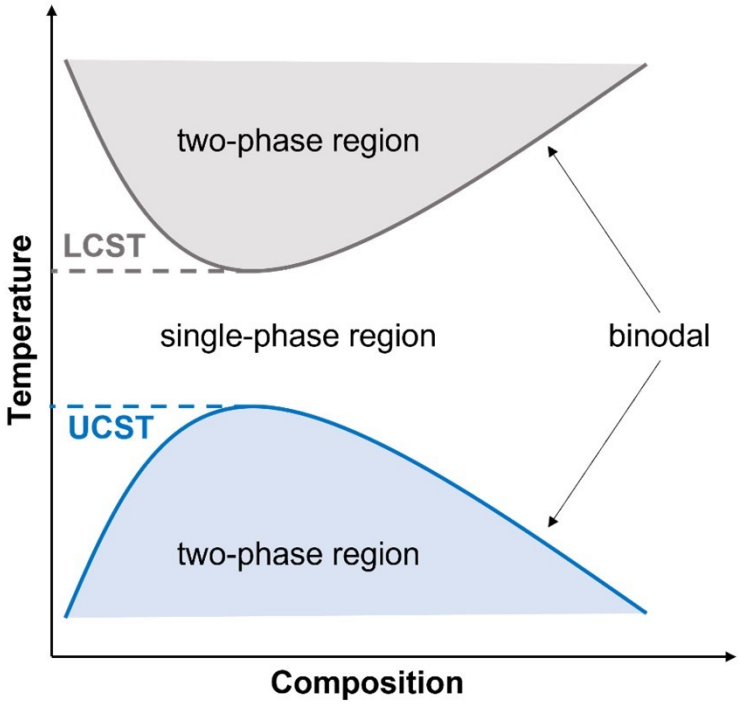

Figure 3: Phase diagram of thermoresponsive polymers solution in water with depicted values of LCST and UCST.

Above (UCST) and belove (LSCT) these transition temperatures, the polymer solution is homogeneous and clear, the polymer is soluble in water.[10, 11] Temperature at which clear, homogenous solution changes to turbid, cloudy one is called a cloud point. The cloud point is concentration dependant. Binodal line in Figure 3 represents the coexistence of single-phase region and two-phase region. The minimum (maximum) on the binodal curve represents LCST (UCST).[10, 11] The separation below UCST is an enthalpy driven process where the contribution of the enthalpy of mixing to the ΔG is greater than the contribution of entropy (Eq. 1). For polymers with LCST, above the transition temperature the conformation changes from random coil to more compact, globular one, minimizing the contact with solvent and the phase separation occurs.[12, 13, 14] This process is entropy driven (Eq. 1). From the Gibbs equation:

$$\Delta G = \Delta H - T\Delta S, \tag{1}$$

where G is Gibbs energy, H is enthalpy, T is temperature and S is entropy, by increasing the temperature the entropy term becomes predominant and phase separation becomes more favourable process. Polymers with LCST are more common than the ones with UCST. [12, 13]

Since its synthesis in 1967 poly(N-isopropylacrylamide), PNIPAM, has been one of the most studied thermoresponsive polymers. PNIPAM exhibits LCST in aqueous solution at around

32 °C, which is in the range of human body temperature. The temperature driven structural change from coil to globule conformation causes release of water from hydration layer of the polymer (Figure 4). The LCST can be optimized by introducing a co-monomer.[13, 15] Copolymerization with hydrophilic segments increases LCST and decreases by copolymerization with hydrophobic segments. PNIPAM microgels and hydrogels are used in drug delivery or biosensing.

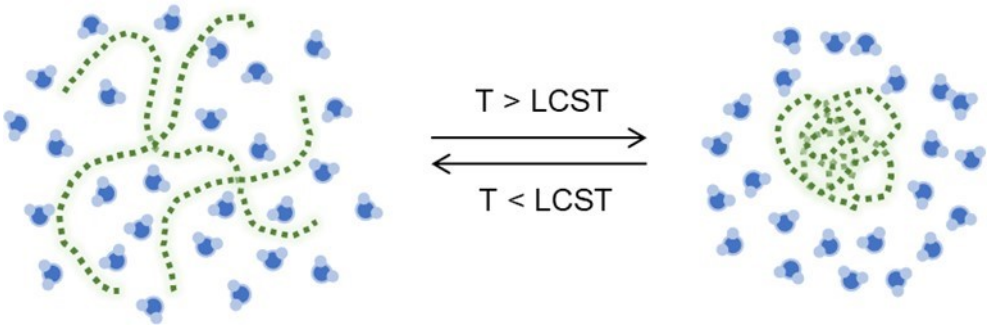

Figure 4: Schematic of structural change of PNIPAM at temperature change. The expanded or collapsed polymer coil is depicted by green line surrounded by water molecules in blue.

2.3.2. pH-responsive polymers

Polymers that reversibly change their solubility, volume, configuration and conformation in dependence of external pH are called pH-responsive polymers. These polymeric systems are applicable in drug delivery. The extracellular pH of tumors is slightly acidic, the release of the drug can be triggered by pH change.[16, 17] Response to pH can trigger variety of changes that depend on structure of the polymer. For example, pH change can cause chain collapse/extension, (de)protonation of functional groups, swelling or micelle formation. pH-responsive polymers contain ionizable pendant groups that can accept or release protons which changes their ionization degree and their net charge. The increase of the net charge causes transition from collapsed to expanded state. On the other hand, decrease of the net charge causes transition from expanded to collapsed state. pH-responsive polymers belong to one of two categories. First, polymers with acidic groups like carboxylic group, sulfonic acid, phosphonic acid or boronic acid. Second are polymers with basic groups like tertiary amine groups, pyrrolidine, pyridine or imidazole groups.[17,18]

Poly(acrylic acid) (PAA) is pH-responsive polymer that at low pH has neutral charge and not fully collapsed globular conformation and at pH around 5 extends to open coil conformation (Figure 5). The chain extension is caused by repulsion of negatively charged groups due to deprotonation at high pH. Copolymers containing PAA are extensively studied

pH-responsive materials, which solubility in aqueous solutions and morphology can be tuned by optimizing the PAA block length, pH and salt concentration.[16, 19, 20]

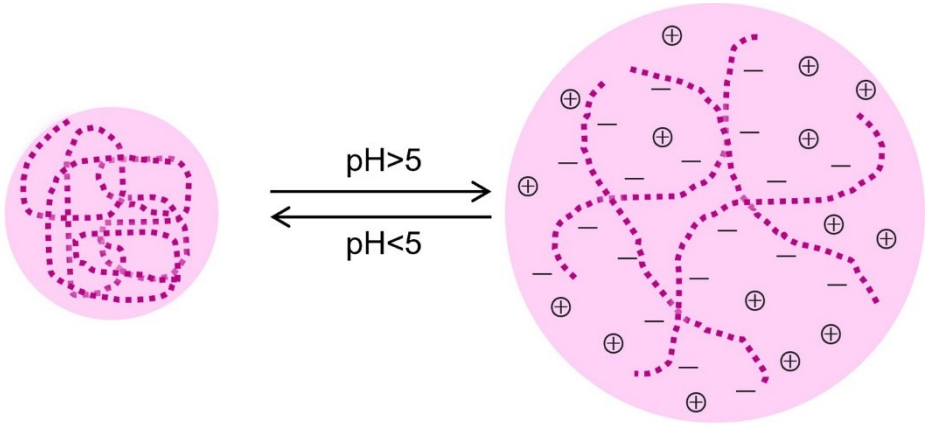

Figure 5: Schematic of swelling of PAA at pH change. The expanded or collapsed polymer coil is depicted by pink line, where expanded coil bears negative charges surrounded by positively charged counterions.

2.4. Triblock copolymer interactions

Block copolymers consist of two or more polymers blocks, where each block consists of the same polymer segments. Block copolymers are useful building blocks in nanochemistry, because their properties can be tuned by optimizing parameters like individual block lengths, their order in sequence or functionalization of end groups.[21, 22] They can be prepared via variety of polymerization techniques from which controlled polymerization like RAFT or ATRP are used most often. Block copolymers can assemble in selective solvents and the resulting nanostructures can be applied in variety of fields like drug delivery, nanoprobes or microreactors.[22, 23] A-B diblock copolymers nanostructures usually have core-shell architecture in selective solvents. Tri- (multiple-) block polymers can form more complex architectures in solutions. Triblock A-B-A can form core/shell micelles in solution in case that B is solvophobic block and A are solvophilic. Other morphologies adopted by A-B-A triblock are lamellas, cylinders or spheres.[22, 24] In the case of triblock B-A-B where B is solvophobic and A is solvophilic, polymers can form flower like micelles if block A is long enough (Figure 6). Triblock terpolymers A-B-C, which consist of three types of segments, can form more complex architectures than A-B-A copolymers and their self-assembly often leads to distinct compartmentalization.[21, 22, 25] In recent years double hydrophilic block copolymers (DHBC) and their co-assembly in solution have been studied. DHBC consist of

two different hydrophilic polymer blocks. Addition of additives like macroions or change in environmental conditions like temperature, pH can lead to formation of nanoparticles.[25, 26, 27]

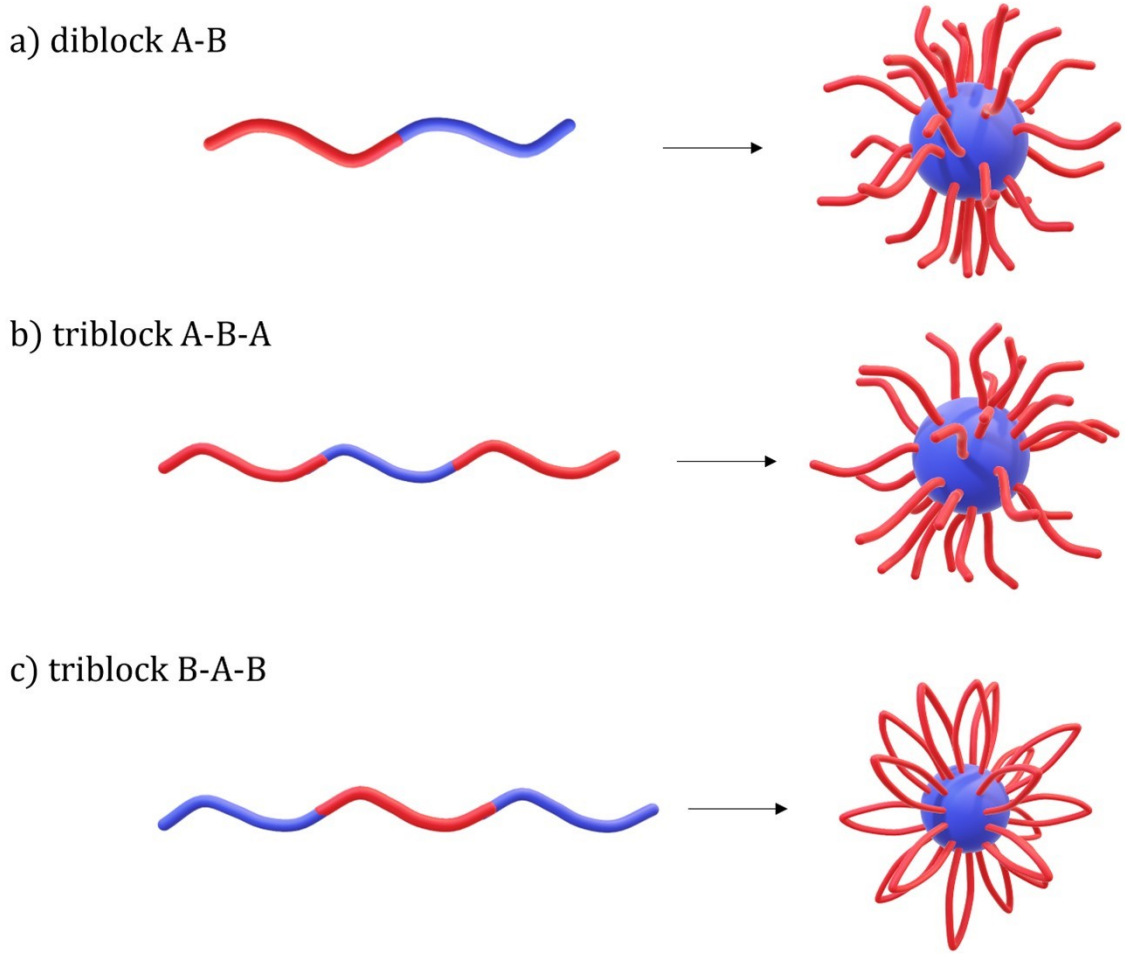

Figure 6: Examples of diblock and triblock copolymer architectures. A (red) is a solvophylic block and B (blue) is a solvophobic block.

By interactions of block copolymers with macroions or crosslinking of polymers 3D nanostructures can form. Nanogels are nanoscale size materials formed by swellable polymer networks.[28, 29, 30] Hydrogels are crosslinked swellable networks that can hold large amount of water. They are mostly hydrophilic materials that have high loading capacity. Gels can have special properties like porosity, degradability, or stimuli responsiveness. The interconnections in gels can be either chemical or physical. Chemical crosslinking is created by covalent bond between polymer chains in presence of crosslinker. These crosslinking mechanisms involve click chemistry, Schiff-base reactions and amide crosslinking among others. Physical crosslinking is stabilized by non-covalent bonding like electrostatic interactions or via weak interactions like hydrogen bonding or hydrophobic interactions.

Among the approaches for creation of physical gels are increasing/decreasing the temperature, changing the pH to form hydrogen bonds, introducing oppositely charged ions into the solution.[28, 29, 30] Once the crosslinking is achieved in gels, they can exhibit viscoelastic behaviour, that can be described by rheology measurements (Section 3.5.). Properties like softness can change under deformation, or self-healing can be observed and measured experimentaly.[31]

Thanks to the ability of gels to incorporate biological molecules and drugs into their structure, gels are suitable materials for drug delivery. Inside the gels, drug is encapsulated into the polymeric network by van der Waals, hydrophobic or covalent bonds. Drugs can be than released by stimuli response of the polymeric network. Further accumulation into targeted tissue can be mediated by functional groups on gel surface. Recently, hydrogels have been tested for the emerging biomedical field of tissue engineering.[31, 32]

3. Characterization techniques

For polymer characterization variety of techniques can be used to get a complex picture of a polymeric system. Nuclear magnetic resonance is often used to determine the polymer structure or kinetics of polymerization. Different scattering methods like light scattering, small-angle X-ray scattering (SAXS) can determine nanoparticle size distribution, size and shape of micelles and other properties such as aggregation number. In recent years, to characterize the structure of nanoparticles in solution cryogenic transmission electron microscopy (cryo-TEM) has been used. Rheology is used for determination and measurement of viscoelastic and mechanical properties.

3.1. Nuclear magnetic resonance

Nuclear magnetic resonance (NMR) is spectroscopic method that has been used for polymer characterization for a long time. NMR provides useful information about polymers like determination of the chemical structure, polymer stereoisomerism (so called tacticity), polymer chain dynamic or molecular weight analysis.[33, 34] The nuclear spin, $\vec{I}$, is fundamental parameter for NMR. It depends on the mass number and atomic number of the nucleus. Nuclei that have zero nuclear spin like ^{12}C, ^{16}O, ^{32}S are not detected. Typical nuclei that are used in polymer NMR experiments are ^{1}H, ^{13}C, ^{15}N or ^{31}P. Nuclei with non-zero nuclear spin have magnetic dipole moment, $\vec{\mu}$, which is related to nuclear spin via following equation,

$$\vec{\mu} = \gamma \cdot \vec{I} \tag{2}$$

where γ is gyromagnetic ratio.[35] In solution NMR, sample is placed into a magnetic field where NMR-active isotopes align according to its *z*-axis. Perpendicularly to this magnetic field is applied weaker magnetic field that rotates the bulk magnetization into the *x, y*-plane. The magnetized sample undergoes Larmor precession that is dependent on magnetic field as well as magnetic moment.[35, 36] The chemical shift is defined as

$$\delta = \frac{\omega - \omega_{ref}}{\omega_{ref}} \tag{3}$$

where ω is frequency of interest and ω_{ref} is frequency of a reference gives the position of the signal in the frequency spectrum. Chemical shift gives information about local environment of the nucleus and is expressed in parts per million (ppm). Chemically

equivalent atoms of the same type have the same local environment and therefore the same chemical shift.[35, 36] NMR spectroscopy in polymer chemistry can be used to study mechanism of polymerization by labelling the initiator with isotopes like ^{13}C. Labelling with NMR active isotopes can also help with analysis of end groups and structural defects of polymers. The kinetics of the polymerization can also be observed as intensity decrease of monomer signals and intensity increase of polymer signals that are generally broader than signal for classical compounds.[35, 36]

3.2. Light scattering

When polarizable particles are placed in the electric field of light a dipole is induced in it with the same oscillation frequency as the incident light in all directions. The overall scattering of a macroscopic system is caused by interference effect of all components.[37] In case of liquids, the scattering is caused by density fluctuations. For colloids, nanoparticles dispersions and polymer solutions, scattering is caused by fluctuations in concentration and the spatial distribution of the scattered light, which is proportional to the size and shape of nanoparticle in the system. An important parameter is scattering angle (θ), it is the angle in between an incoming beam of light and scattered one. The two main approaches of the light scattering measurement are: dynamic and static light scattering.[37, 38, 40]

In the static light scattering (SLS) the instrument collects average intensity of the light that is scattered by sample with certain concentration at the certain angle. The difference between wave vectors of the incident light and scattered light is called scattering vector $\vec{q}$. Magnitude of scattering vector can be expressed by the equation:

$$q = \frac{4\pi n}{\lambda} \sin\frac{\theta}{2} \tag{4}$$

where λ is the wavelength of the incident light, n is refractive index of the medium and θ is the scattering angle. Data from SLS are often treated by Zimm equation, which provides information about weight average molar mass, radius of gyration or structure factor.[37, 38]

Dynamic light scattering (DLS) is based on the premise that the scattering particles present in a solution move according to Brownian motion. Fluctuations in light scattering caused by either absorption or scattering (or both) and are collected by the instrument. These fluctuations provide the information about the size and diffusion coefficient of the measured

system. In a medium where Brownian motion is limited, for example in gels or glasses, where positions of scatters are fixed, the scattering is caused by density fluctuations.[37, 38, 39]

In DLS experiment an intensity-time autocorrelator monitors scattering intensities in small time intervals τ over a total observation time t. The intensity correlation function $G_2(\tau)$ is measured and can be expressed as

$$G_2(\tau) = \langle I(t)I(t+\tau)\rangle \tag{5}$$

where $(t + \tau)$ is delayed time. This intensity correlation unction can be normalised and determined as

$$g_2(\tau) = \frac{\langle I(t)I(t+\tau)\rangle}{\langle I(t)\rangle^2}. \tag{6}$$

The DLS data analysis can be done by two methods depending on the properties of the system. Cumulant method is appropriate for the system which is monomodal. This method gives the diffusion coefficient (z-average), D_Z, from which its radius can be calculated. Particles with bigger diffusion coefficient are moving quickly and are smaller in size corresponding to the fluctuations in scattering intensity.[37, 38, 40] Diffusion and size of the spherical particle is expressed in Stokes-Einstein equation:

$$D = \frac{k_B \cdot T}{6\pi\eta R} \tag{7}$$

where T is the absolute temperature, η is dynamic viscosity, k_B is the Boltzmann's constant and R is the radius of the spherical particle. By rearranging the Stokes-Einstein equation hydrodynamic radius R_H, which also takes into account the hydration shell of the micelle can be calculated using experimentally measured value D_{exp}

$$R_H = \frac{k_B \cdot T}{6\pi\eta D_{exp}}. \tag{8}$$

To obtain the true value of D_z, the experimentally obtained values are extrapolated to $\theta = 0°$ and concentration $c = 0$ g/L, which is usually expressed as dynamic Zimm plot.[40, 41]

The second method is constrained regularization method (CONTIN) and it is more appropriate for polymodal systems. In polydisperse suspension correlation function cannot be represented as a single exponential, but it can be expressed as an integral over the decay

rate. The CONTIN method involves inverse Laplace transformation, which provides distribution of hydrodynamic radii by implementation of Stokes-Einstein equation.[42]

3.3. Size exclusion chromatography

Size exclusion chromatography (SEC) is separation technique based on separation of materials according to their molar mass. The basic principle is the diffusion of dissolved molecules into the pores of various sizes in the gel that makes up the stationary phase. The stationary phase is represented by a pore filled with a solvent within porous gels that can be hydrophilic or hydrophobic, and is chosen according to the used solvent. Smaller macromolecular coils enter the pores in higher extent than bigger macromolecules. The bigger the elution volume the smaller the particle. SEC uses variety of detectors such as refractometric (combined with spectrophotometric one), viscosimetric or light scattering.[43, 44, 45]

SEC chromatograms provide distribution functions of molar masses, and their average values M_n and M_w:

$$M_n = \sum_i x_i \cdot M_i \tag{9}$$

$$M_w = \sum_i w_i \cdot M_i \tag{10}$$

where M_n is number average molar mass, x_i is mole fraction of molecules with molar mass M_i and M_w is weight average molar mass, w_i is weight fraction of molecules with molar mass M_i. Another important characteristic obtained from SEC is dispersity $Đ$, which describes uniformity of polymer sample.[43, 44, 45] Dispersity can be calculated using equation:

$$Đ = \frac{M_w}{M_n}. \tag{11}$$

3.4. Fluorescence spectroscopy

Fluorescence is a photon emission due to a spontaneous spin-allowed transition from the excited state S_1 to ground state S_0. Jablonski diagram (Figure 7) summarizes all the processes that influence fluorescence on the level of electronic and vibrational states. Fluorescence concerns mainly species that are rich in energy (fluorophores) and are able to interact with their surroundings.[40, 46, 47] Fluorophore is incorporated into a system of interest which yields information about said system. Systems with intrinsic fluorophore like proteins containing

tryptophan are inherently luminescent. But this is not a case for many macromolecules, therefore an extrinsic fluorophore probe needs to be added to the system in concentration about 10^{-6} M. The choice of fluorophore is important because it has to be able interact with the host system.[40, 46, 47]

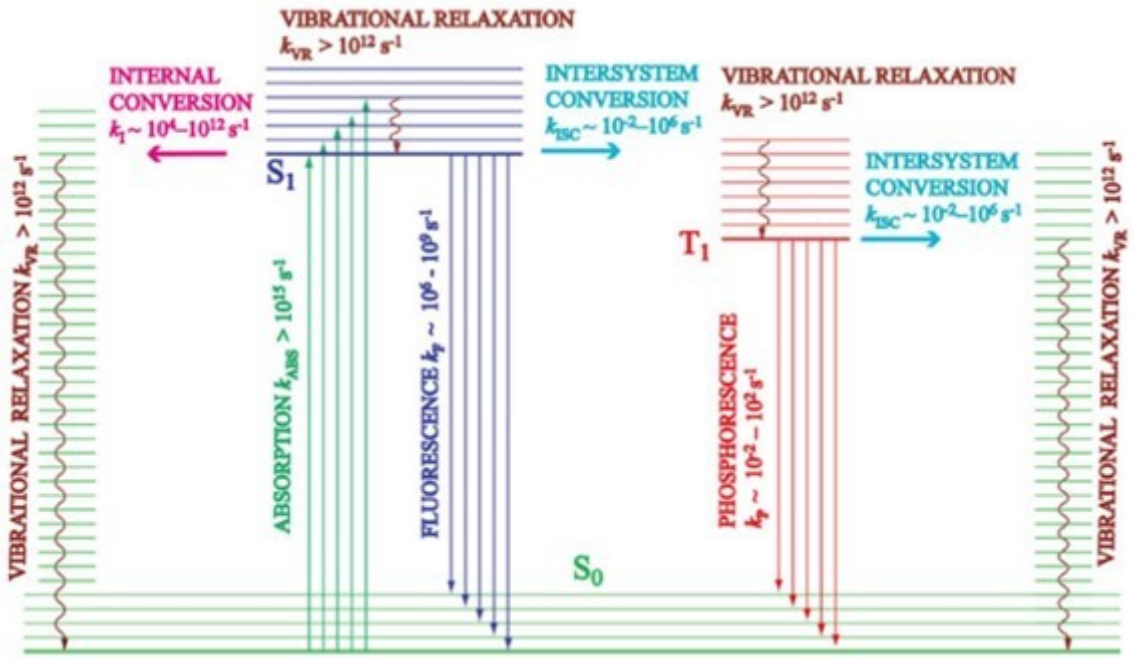

Figure 7: Jablonski diagram describing possible photophysical processes with their typical rates; scheme taken form Ref. 46.

Molecule in the lowest vibrational state of the lowest electronic state, S_0 is excited by photon absorption to higher excited state, S_1. The condition for excitation, that the internuclear distances stay unchanged is described by Franck-Condon principle. The molecule goes to lower vibrational state within the existed state because of the vibrational relaxation. The relaxation to ground state can be achieved by either non-radiative or radiative processes. The non-radiative processes are vibrational relaxation, internal conversion and intersystem crossing. The spin-allowed photon emission from S_1 to S_0 is fluorescence.[46, 48, 49]

Before excitation fluorescent probe is randomly oriented in solution. Immediately after excitation, excited molecules with absorption dipole moment parallel to excitation polarization dominate. Due to Brownian motion of the fluorophore molecules and excitation energy migration, the anisotropic orientation of the excited molecules starts to relax.[40, 46, 50] Measurement of this relaxation is possible due to time-resolved fluorescence anisotropy defined as:

$$r(t) = \frac{I_{\parallel}(t) - I_{\perp}(t)}{I_{\parallel}(t) + 2I_{\perp}(t)} \quad (12)$$

where $I_{\parallel}(t)$ is the parallely polarized and $I_{\perp}(t)$ is perpendicularly polarized fluorescence intensity with respect to the excitation pulse. In solutions, the rotational diffusion proceeds at the timescale comparable to the fluorescence decay and can be used to study the viscosity of the microenvironment.[46, 50]

In polymer chemistry, fluorescence spectroscopy measurements are used for studying of integration and release of fluorescent probe, its microenvironment or mobility, which are useful information for potential application in drug delivery. [48, 49]

3.5. Rheology

Rheology is science of flow and deformation of bulk materials as it was described in more than 70 years ago. The ideally elastic material stores the deformation energy as internal energy after applying force and after removal of the force energy is released. Ideally plastic/viscous material consumes the deformation energy, and the energy is lost as heat after applying force. In glassy polymers or rigid networks, the elasticity (storage modulus G') is caused by enthalpy spring mechanism.[51, 52, 53] In permanently or physically crosslinked flexible 3D networks the elasticity is caused by entropy spring mechanism. Plasticity (loss modulus G'') in flexible materials is caused by molecular friction between polymer chains. In stiffer and rigid networks the plasticity is caused by reorganization of morphology, migration of defects or reorientation of crystalline domains.[51, 52, 53] Different moduli are used to characterize elasticity for different types of deformation. Young´s modulus, *E,* describes deformation by elongation ε

$$\sigma = \varepsilon \cdot E, \quad (13)$$

where σ is stress. Compression modulus, *K*, describes deformation by volume compression $\frac{dV}{V}$

$$dp = -\frac{dV}{V}K, \quad (14)$$

where *dp* is change in pressure. Shear modulus, *G*, describes deformation by shear γ

$$\sigma_T = \gamma \cdot G, \tag{15}$$

where σ_T is shear stress. Model that describes the ideally elastic material is the ideal spring and ideally viscous material can be described by the dashpot model (Figure 8).

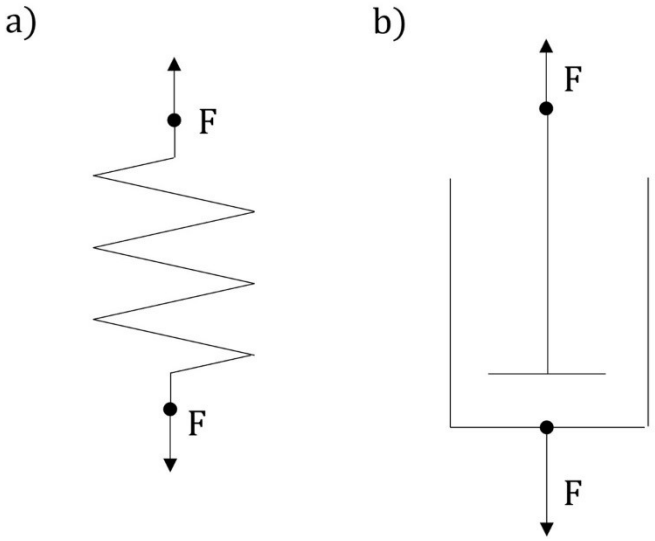

Figure 8: Schematic of a) spring model for elastic materials and b) dashpot model for viscous materials.

The real materials combine viscous behaviour of liquid and elastic behaviour of solids. Viscoelastic materials can be described by variety of models that combine two or more elements. Many tests have been developed to analyse viscoelastic behaviour. Among those the oscillatory experiments are well suited to describe both viscoelastic liquids and solids. Amplitude sweep is a simple test where deformation amplitude is gradually increased and crosslinking in the sample is disconnected via mechanical work. The storage and loss modulus are plotted against deformation. Frequency sweep measurements are made at different oscillation frequencies at the constant amplitude. The storage and loss modulus are plotted against frequency to analyse sample behaviour at slow and fast changes of stress. [51, 52, 53]

Non-Newtonian fluids cover a wide range of materials that depart from classical Newtonian behaviour in their ability to shear thin or thicken, creep or stress relax. Rheology focuses on five main groups of non-Newtonian fluids: shear-thinning, shear-thickening, thixiotropic, rheopectic fluids and Bingham plastics. Shear thinning materials undergo viscosity decrease with increasing shear rate due to disentanglement of crosslinking. Many linear polymers belong to this group apart from materials like glue or coatings. On the other hand, viscosity of shear thickening materials increases with shear rate.

Microgels and suspensions with a high content of solid matter show shear thickening behaviour due to the aggregation or percolation of molecules. Pure polymers that are branched but not cross-linked which can lock entanglements also have this tendency.[51, 54]

3.6. X-ray scattering techniques

X-ray scattering techniques are generally non-destructive techniques used for characterization of nanoparticles with nonuniform particle size. These techniques directly provide the averaged particle size. Their scattering is weaker due to the small volume and small size of nanoparticles compared to bulk materials. Signal can be increased if sample is measured for longer time. Both small-angle X-ray scattering (SAXS) and wide-angle X-ray scattering (WAXS) use the electron density of the sample to provide information about it. SAXS analysis typically runs at angles between 0.1 and 10°, WAXS uses angles wider than 10°.[47, 55, 56]

SAXS is a powerful method for determination of particle size, their distribution and shape averaged over macroscopic sample volume at nanoscale resolution. SAXS typically uses multiple types of detectors that output two-dimensional (2D) scattering pattern. 2D data is converted into the one-dimensional (1D) scattering curve. The scattering profile is a plot of the scattering intensity against the variable q (Equation 4).[55, 56, 57] SAXS signal is derived from the difference in average electron density of sample molecules, $\rho(r)$ and bulk solvent ρ_S,

$$\Delta\rho(r) = \rho(r) - \rho_S. \tag{16}$$

SAXS profile, where scattering intensity is plotted versus q, can be split into two components including the form factor $P(q)$, which provides information about the mean structural properties of the individual particles (size, shape, internal structure), and the structure factor $S(q)$, that provides information about interactions with neighbouring particles. In SAXS profile the lowest resolution portion, which describes the individual particles gives information about radius of gyration R_G.[47, 55, 56]

4. Aims of the thesis

This thesis is a contribution to the long-term study of boron-rich nanoparticles and nanomaterials formed by block copolymers and boron cluster compounds in the Soft Matter research group, Department of Physical and Macromolecular Chemistry. The aims of this thesis are following:

1. To prepare stable hydrogels by electrostatic interaction of polycationic A-B-A triblock copolymer poly(2-(N, N, N′, N′-tetramethyl guanidinium) ethyl acrylate)-*b*-poly(ethylene oxide)-*b*-poly(2-(N, N, N′, N′-tetramethyl guanidinium) ethyl acrylate) with sodium *closo*-dodecaborate anion, and to study their properties by variety of rheology, scattering and spectroscopy techniques.
2. To prepare thermoresponsive gels by dihydrogen bonding of polyanionic A-B-A triblock copolymer poly(N-isopropylacrylamide)-*b*-poly(acetic acid)-*b*-poly(N-isopropylacrylamide) with sodium [cobalt(3+) 1,2-bis(dicarbollide)] and to study their properties by variety of rheology techniques.
3. To study the impact of diverse salts on the formation and stability of the nano-complex of poly(ethylene oxide) with sodium and lithium [cobalt(3+) 1,2-bis(dicarbollide)] in aqueous solutions.

The obtained pieces of knowledge will allow for reproducible preparation of stable boron-rich nanomaterials and deeper understanding of gelation and complexation processes induced by anionic boron cluster compounds.

5. Materials and methods

5.1. Used polymers and other reagents

PGEA-PEO-PGEA systems

Polymers poly(2-(N, N, N′, N′-tetramethyl guanidinium) ethyl acrylate)-*b*-poly(ethylene oxide)-*b*-poly(2-(N, N, N′, N′-tetramethyl guanidinium) ethyl acrylate), $PGEA_{20}$-PEO-$PGEA_{20}$ (M_n= 21.7 kg/L, $Đ$ = 1.14) and $PGEA_{40}$-PEO-$PGEA_{40}$ (M_n= 33.5 kg/L, $Đ$ = 1.09), with PEO (M_n = 10 kg/L) were synthesized via RAFT polymerization by M. Sc. Jianwei Li, Ph.D, Synthetic route is presented in Figure 9.

Sodium *closo*-dodecaborate (anhydrous), $Na_2[B_{12}H_{12}]$, was purchased from KatChem Ltd., Czech Republic, and used without further purification.

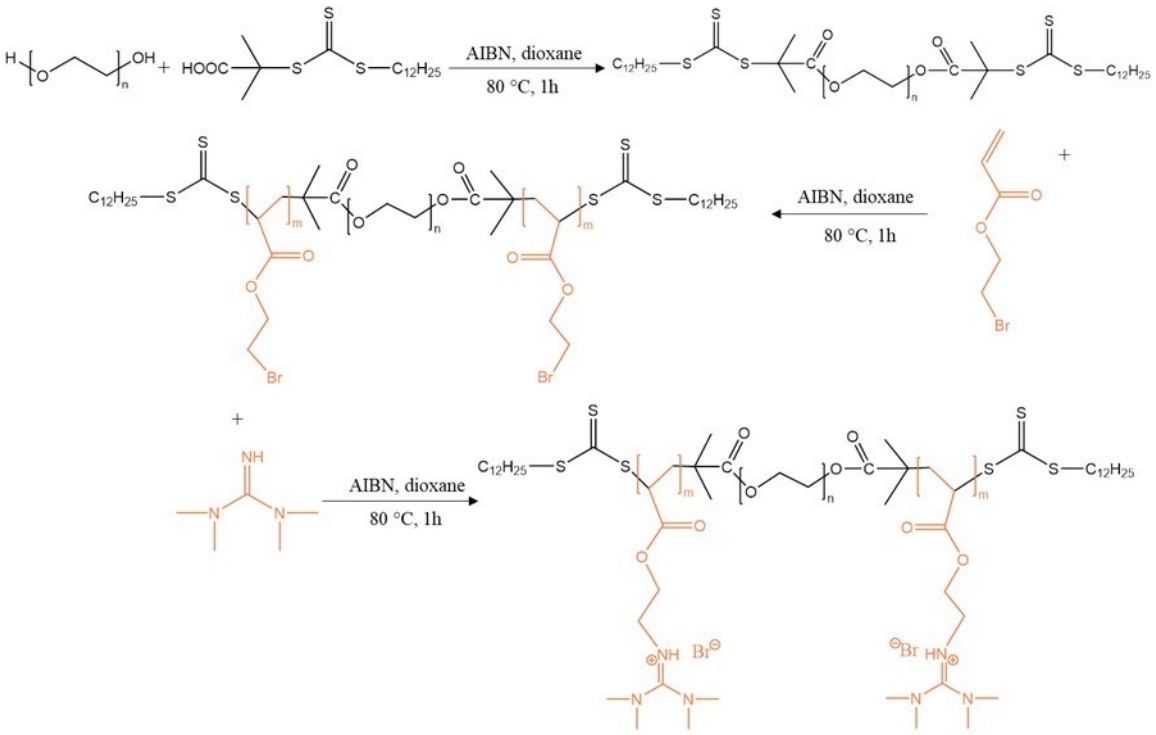

Figure 9: PGEA-PEO-PGEA synthetic route done by RAFT polymerization.

PNIPAM-PAA-PNIPAM systems

N-Isopropylacrylamide ≥ 99%, *tert*-Butyl acrylate, trifluoroacetic acid ≥ 99%, dichlormethane, dioxane, diethyl ether, methanol, ethanol, toluene, 2,2′-Azobis(2-methylpropionitrile) (AIBN) were purchased from Merck (Figure 10).

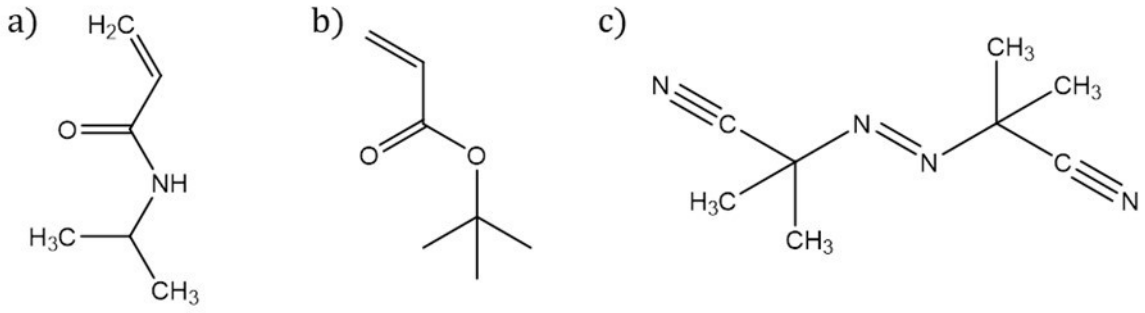

Figure 10: Monomers and initiator used for RAFT polymerization: a) NIPAM, b) tert-butyl acrylate, c) AIBN.

N-Isopropylacrylamide monomer was recrystallized from toluene, *t*-butyl acrylate monomer was passed through a column, with stationary phase neutral Al_2O_3, with pore size 58 Å. AIBN initiator was recrystallized from ethanol.

PEO/COSAN systems

Poly(ethylene oxide) M_n = 20 kg/L was purchased from Merck (Figure 11).

Pure salts: sodium fluoride, sodium chloride, sodium iodine, sodium sulfate, sodium thiocyanate, lithium fluoride, lithium chloride, lithium iodine, lithium sulfate and lithium thiocyanate with undetermined amount of water were also purchased from Merck (Figure 11).

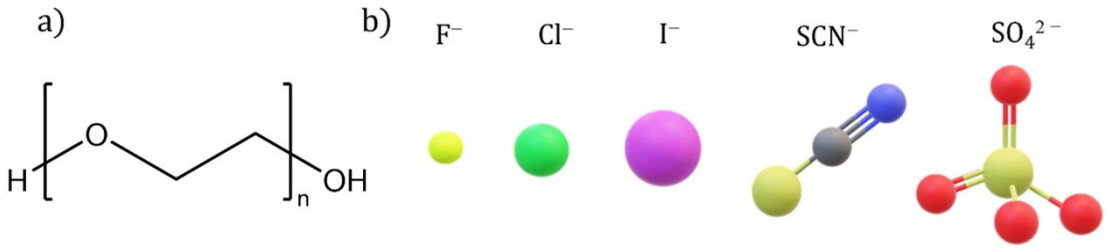

Figure 11: Polymer and salts used: a) PEO, b) anions of MF, MCl, MI, MSCN and M_2SO_4 salts where M = Li, Na.

Cesium [3-cobalt(3+) 1,2-bis(dicarbollide)], Cs[COSAN], was purchased from Katchem Ltd., Czech Republic, and used without further purification. Cation exchange of Cs[COSAN] to Li[COSAN] and Na[COSAN] is following. Firstly, the resin was charged by passing 250 mL of 3M HCl and then rinsed with water. Next, the column was loaded with desired cations M (lithium or sodium respectively) by passing 3M MCl solution through resin, and then rinsing with around 500 mL of water until the pH was neutral (the eluent was tested to see if it contains traces of MCl by AgNO3 solution). Solid Cs[COSAN] was dissolved in a mixture of acetonitrile/water (50:50) and this solution (around 100 mL) was passed repeatedly through (drop by drop) a cation exchanging resin loaded with the desired cation. The solvent was finally evaporated, and the crude product was left to dry in a desiccator overnight.

5.2. Nuclear magnetic resonance

^{1}H NMR spectra were measured on a Varian ^{UNITY}*INOVA* 400 in chloroform-d and deuterium oxide (99.8 %; Chemotrade, Leipzig, Germany).

5.3. Size exclusion chromatography

Size exclusion chromatography (SEC) was performed at 55 °C in N,N-dimethylacetamide (DMA) containing 50 mM of LiCl at an elution rate of 0.5 ml·min^{-1} using a Watrex Streamline system equipped with a Streamline P1 Pump, a Streamline AS2 Autosampler, a Streamline CT1 Column Thermostat, a Streamline UV1 detector, and a Streamline RI1 detector. The separation was performed on two PLgel 5 μm mixed-D columns in series. Molar masses and dispersities were calculated against PMMA standards. Samples were filtered using PTFE filter before injection

5.4. Dynamic light scattering

The dynamic light scattering measurements were performed on photometer (ALV, Germany) consisted of CGS-3 automatic goniometer, a 7004 multitau multibit autocorrelator, two high-QE APD pseudo cross-correlation detectors, and a 100 mW, 660 nm diode-pumped solid-state laser (Cobolt AB, Sweden). Dynamic light scattering was performed at for the scattering angles ranging from 50° to 150°. Measurement were carried out at different temperatures from 20 °C to 60 °C. DLS data analysis was performed by

fitting the measured normalized intensity autocorrelation function $g_2(t) = 1 + \beta|g_1(t)|^2$, where $g_1(t)$ is the electric field correlation function, t is the lag time and β is a factor accounting for deviation from the ideal correlation. DLS analysis by CONTIN method provides the distribution of relaxation times, $\tau A(\tau)$. Before measurement samples were filtrated through membrane filters.

5.5. Rheology

Rheology measurements were performed using an Anton-Paar MCR 501 rheometer with a cone–plate stainless steel geometrical setup. A 25 mm upper rotating cone plate with cone angle 1° was used for all measurements with constant gap size of 0.048 mm. The measurements were conducted at room temperature 25 °C. The samples were allowed to reach temperature equilibrium for 4 minutes prior to each measurement. Measurements for thermoresponsive systems were done at temperatures 20, 32, 36 and 40 °C.

5.6. Fluorescence spectroscopy

Time-resolved measurements were performed using PicoQuant FluoTime 300 fluorimeter (PicoQuant GmbH, Germany), equipped with a pulsed laser diode LDH-470DC (PicoQuant) with excitation wavelength 470 nm, was used to excite the sample and mounted directly on the sample chamber at 90°. The photons were collected by a PMA Hybrid-40 detector (PicoQuant). The data were acquired and analysed by using the commercially available software EasyTau II (PicoQuant GmbH, Germany). For fluorescence measurement was used newly synthesized fluorescence probe fluorescein- dodecaborate conjugate FBC (prepared by M. Sc. Jianwei Li, Ph.D).[58] Stock solution with concentration 1 g/L in pure water was used for time-resolved anisotropy measurements.

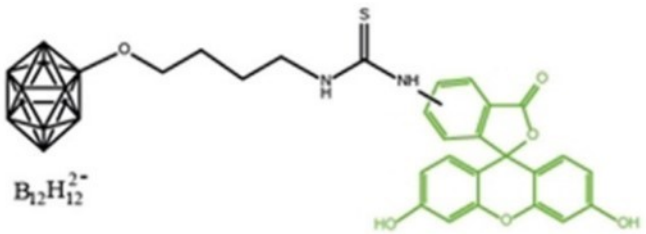

Figure 12: Newly synthesized fluorescence probe – fluorescein-dodecaborane anion conjucate (FBC). Structure taken from Ref. 58.

5.7. Small-angle X-ray scattering

The SAXS experiments were performed using a pinhole camera (modified molecular metrology system) (Rigaku, Japan) attached to a microfocused X-ray beam generator (Rigaku MicroMax 003) operated at 50 kV and 0.6mA (30 W). The camera was equipped with a vacuum compatible version of Pilatus3 R 300 K hybrid photon-counting detector. A setup upgrade made by SAXSLAB enabled the detector to stay aligned with the beam. Three different sample-to-detector distances (namely 1400, 950 and 350 mm) were used to cover a wider q-range. The scattering vector, q, is defined as $q=(4\pi/\lambda)\sin(\theta)$, where λ = 1.54 Å is the radiation wavelength and θ is the scattering angle. The typical exposure time used was 7200 s.

6. Results and Discussion

6.1.PGEA-PEO-PGEA

Triblock copolymers $PGEA_{20}$-PEO-$PEGA_{20}$ and $PGEA_{40}$-PEO-$PEGA_{40}$, with M_n(PEO block) = 10 kg/mol consist of guanidinium functionalized blocks that interact with *closo*-dodecaborate anion $[B_{12}H_{12}]^{2-}$ via electrostatic interactions,[58] and it results in formation of hydrogels at high polymer concentrations with PGEA/dodecaborate nanodomains interconnected by PEO blocks. In this chapter PGEA20 and PGEA40 refer to system $PGEA_{20}$-PEO-$PEGA_{20}$/dodecaborate and $PGEA_{40}$-PEO-$PEGA_{40}$/dodecaborate, respectively. The content of water in gel with the polymer concentration 150 g/L is approximately 85 w-%. The presence of salt in the solution, in this case NaCl, has an impact on properties of the formed hydrogels since salt influence the interaction of dodecaborate and guanidinium functionalized blocks.[58]

Gelation point and segmental dynamics of the gels were investigated by dynamic light scattering. The mobility and microenvironment of dodecaborate clusters within the gel were investigated by fluorescence spectroscopy measurements at J. Heyrovský Institute of Physical Chemistry in Prague with help of Mgr. J. Sýkora, Ph.D.. Mechanical and self-healing properties of the gels were studied by rheological measurements at TU Berlin in the laboratory of Prof. Michael Gradzielski. For determination of the nano-domains size, X-ray scattering measurements were performed and provided by Ing. Jiří Brus, Dr., Institute of Macromolecular Chemistry in Prague.

6.1.1. DLS

Gels from triblock copolymers with two different block lengths (20 and 40 units in PGEA block) were prepared by an addition of sodium dodecaborate into polymer solution in pure water (Table 1). Molar ratio of PGEA segments to dodecaborate anion was set to theoretical electroneutral value of 0.5. Immediately after dodecaborate addition, we could observe that both polymer solutions turned to gels (Figure 13). Samples were left to equilibrate for 1 day before starting the measurement. By dilution of these gels, we can lower their viscosity and obtain honey-like systems and even low-viscous solutions, which probably contain dispersed nanogels and separate flower like micelles (Figure 6c).

Table 1: Sample preparation for DLS experiments, where w % ($P+B_{12}$) is weight percentage of polymer and dodecaborate in sample, m(P) is weight of the polymer and $m(B_{12})$ is weight of the dodecaborate, and the rest is pure water. Visual description is for samples with polymer concentration 150 g/L which was the starting point of the DLS measurement. Volume of the sample for concentration 150 g/L was 500 µL.

Sample	***w* % ($P+B_{12}$)**	***m*(P) [mg]**	***m*(B_{12}) [mg]**	**visual description *c* = 150 g/L**
PGEA20	14.98	75	12.96	gel
PGEA40	15.51	75	16.8	gel

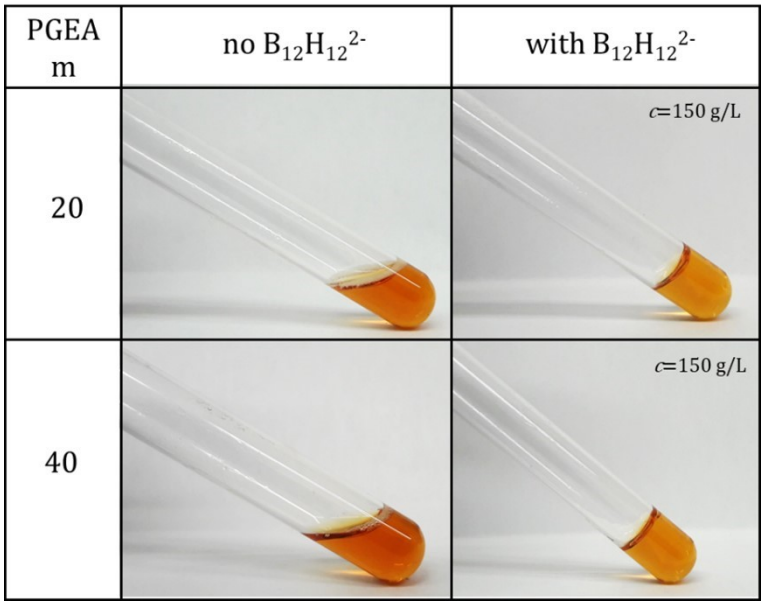

Figure 13:Photographs of samples used for DLS. On the left side are samples with polymer concentration 150 g/L without dodecaborate. On the right side are the same samples but after addition of dodecaborate.

To investigate the point of gelation and mobility of the PGEA-PEO-PGEA polymer segments, a simple DLS experiment was performed with broad concentration range. Measurement started with polymer concentration 150 g/L and concentration was gradually lowered by 1 g/L until a sample with polymer concentration 1 g/L was reached. The dilution of the polymers by pure water was controlled by weight. For the gels, the run time was set as long as 1 hour. Autocorrelation functions were measured at angle 50°, 90°, 130° and 150°. In Figure 14 and Figure 15, there are presented normalized autocorrelation functions at 90°.

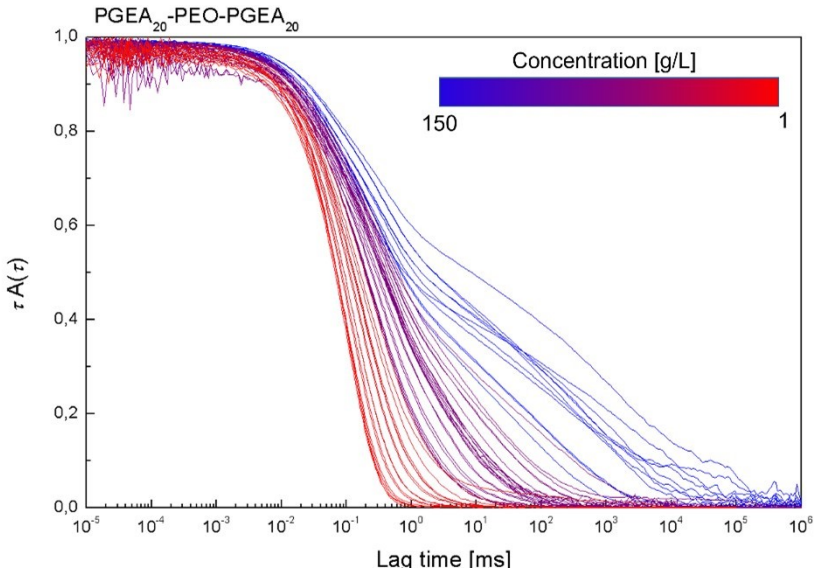

Figure 14: Normalized autocorrelation function of system $PGEA_{20}$-PEO-$PGEA_{40}/B_{12}H_{12}$ at the range of concentrations from 150 to 1 g/L.

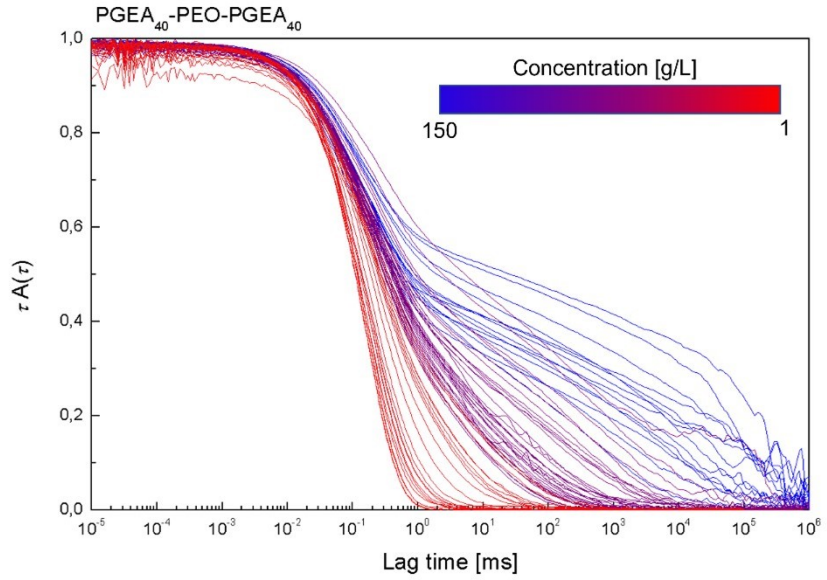

Figure 15: Normalized autocorrelation function of system $PGEA_{20}$-PEO-$PGEA_{40}/B_{12}H_{12}$ at the range of concentrations from 150 to 1 g/L.

For the highest concentrations a distinct slow mode is observed given by internal dynamics of domains within the gel (blue curves in Figures 14 and 15). By dilution, the gel split into separate nanogels and flower micelles that can freely move in solution (red curves in Figures 14 and 15). The transition to freely moving particles is observed earlier for shorter PGEA block with 20 units than for longer blocks. For the PGEA20 samples slow mode starts to disappear around concentration 140 g/L, for the PGEA40 sample around concentration 125 g/L.

6.1.2. Rheology

For both PGEA-PEO-PGEA copolymers, the samples of polymer concentration 150, 147, 142, 139 and 135 g/L in pure water and in 0.1 M NaCl solution were prepared. The PGEA segment to dodecaborate molar ratio was 0.5 (Table 2). Samples were left to equilibrate for 1 day before starting the measurement. The volume of samples was 200 μL.

Table 2: Sample preparation for rheology and their visual description, where c(P) is concentration of polymer, w % (P+B_{12}) is weight percentage of polymer and dodecaborate in sample, m(P) is weight of the polymer and m(B_{12}) is weight of the dodecaborate in pure water and 0.1 M NaCl solution.

PGEA m	*c* (P) [g/L]	*w* % (P+B_{12})	*m*(P) [mg]	*m*(B_{12}) [mg]	visual description
20	150	14.98	30	5.21	gel
	147	14.73	29.4	5.12	gel
	142	14.33	28.4	5.02	gel
	139	14.08	27.8	4.97	honey
	135	13.72	27	3.40	high η solution
40	150	15.51	30	6.71	gel
	147	15.27	29.4	6.64	gel
	142	14.86	28.4	6.47	gel
	139	14.60	27.8	6.39	gel
	135	14.26	27	4.78	honey

Amplitude sweep (Figure 16) was carried out first to determine linear viscoelastic region. For both PGEA20 and PGEA40 samples with the concentrations 150, 147 and 142 g/L, values of G'-storage modulus were higher than values of G"-loss modulus, they are more solid-like. The lowest concentration for both samples show higher G" than G', they are more liquid-like.

For samples containing 0.1 M NaCl (Figure 17) the values of both storage modulus and loss modulus are lower in comparison to samples without added NaCl. For the lowest concentrations in both samples, values of G' and G" are fluctuating, mainly the values of G', because of the lower viscosity of the sample. For both PGEA40 and PGEA20 samples in salt solution with concentrations 150 g/L, and for PGEA40 sample in salt solution for the concentration 147 g/L, values of G' were higher than values of G", they are more solid-like. The lower concentrations for both samples show higher G" than G', they are more liquid like.

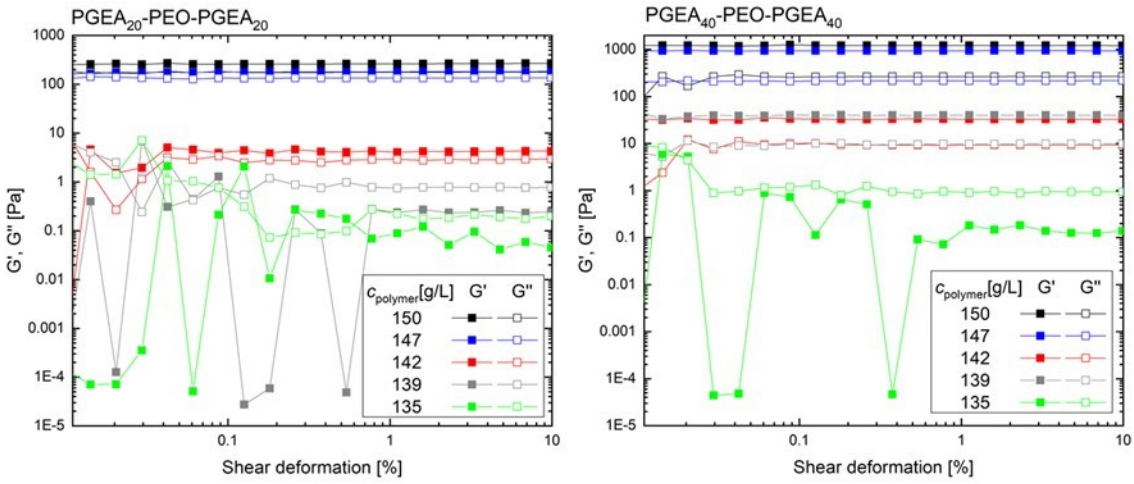

Figure 16: Amplitude sweep for PGEA20 and PGEA40 samples at concentrations 150, 147, 142, 139 and 135 g/L in pure water, where G' is storage modulus and G'' is loss modulus.

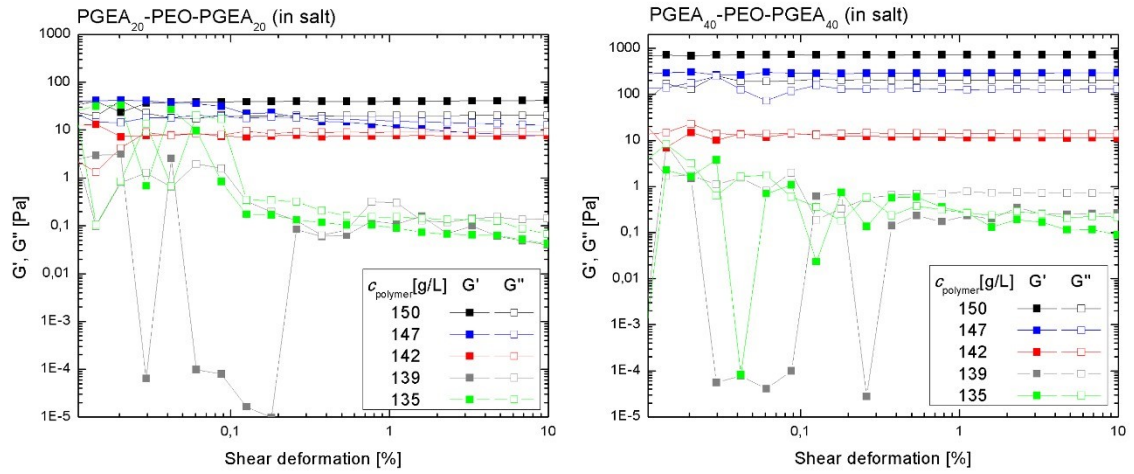

Figure 17: Amplitude sweep for PGEA20 and PGEA40 samples at concentrations 150, 147, 142, 139 and 135 g/L in 0.1 M NaCl solution, where G' is storage modulus and G'' is loss modulus.

Frequency sweep (Figure 18) was carried out at 1% strain, determined from amplitude sweep. In the first step, the frequency goes from low to high values, in the second step it goes from high to low values. For frequency higher than 100, the values of G' and G'' were very unstable and are not shown in the plots. In the frequency region from 1 to 100 Hz, the values of G' and G'' are very similar for both steps of the measurement. Also, in this region G' is higher than G'' for concentrations 150, 147 and 142 g/L, for the concentration 135 g/L G' is lower than G''. For the polymer concentration 139 g/L for PGEA 20 sample, G' is lower than G'', for PGEA40 sample it is the opposite. Below the frequency 1 Hz, there is a difference for G' and G'', these differences are more significant for sample PGEA20. These differences could be caused by sample slipping, by changes in electrostatic interactions within the PGEA/dodecaborate domains or by water evaporation. For the lowest

concentrations in both samples, values of G' and G" are fluctuating, mainly the values of G', because of the low viscosity of the sample. By comparing PGEA20 to PGEA40 samples, we see that storage modulus is lower for PGEA20, this samples form weaker gels than PGEA40.

For samples in 0.1 M NaCl solution, (Figure 19) the values of storage modulus and loss modulus are again lower compared to samples in pure water. We also observe more fluctuations for samples with polymer concentrations 139 and 135 g/L. For sample PGEA20 G' is higher than G" only for concentration 150 g/L. For sample PGEA40, G' is higher than G" for concentrations 150 and 147 g/L.

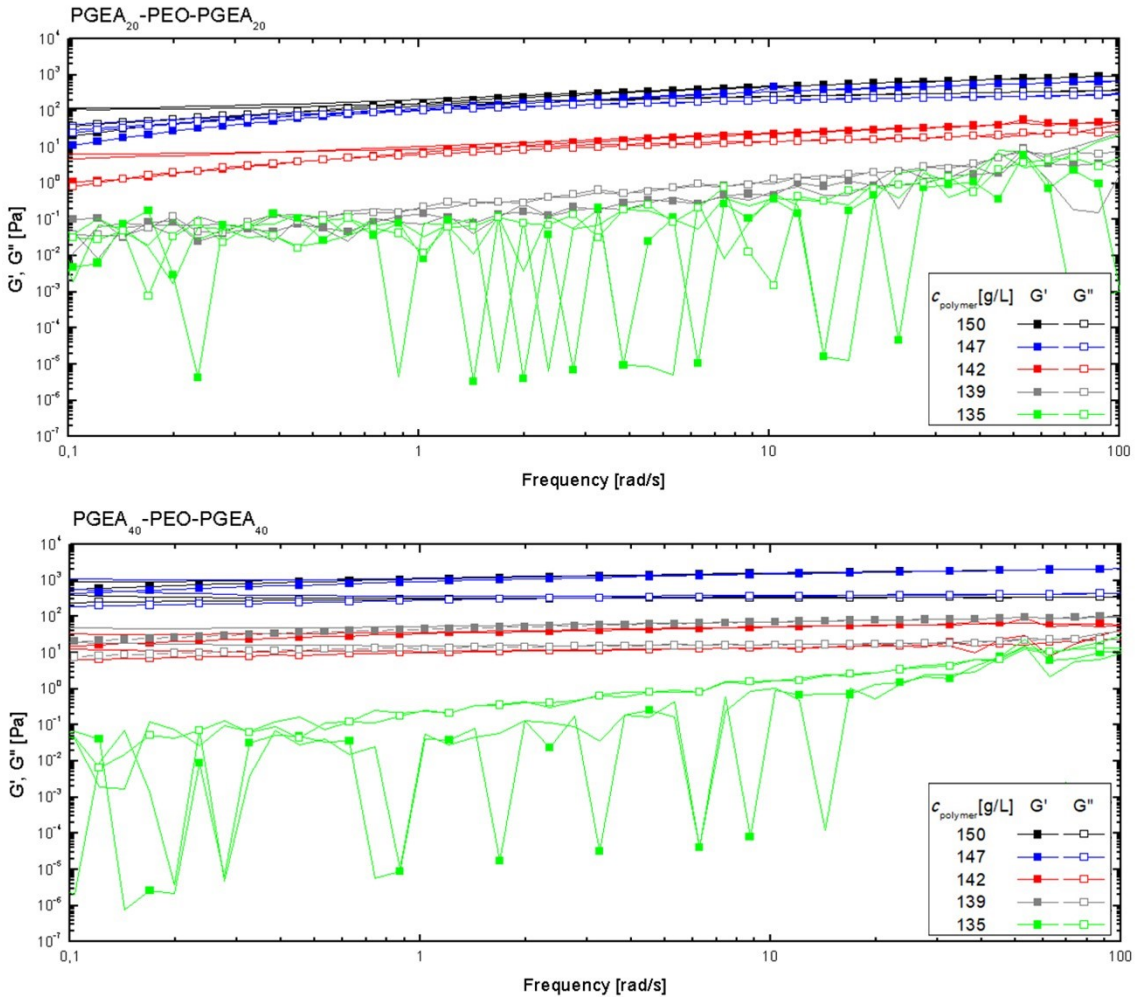

Figure 18: Frequency sweep for PGEA20 and PGEA40 samples at concentrations 150, 147, 142, 139 and 135 g/L in pure water, where G' is storage modulus and G" is loss modulus. 1. step is represented by line and symbol, 2. step is represented by line.

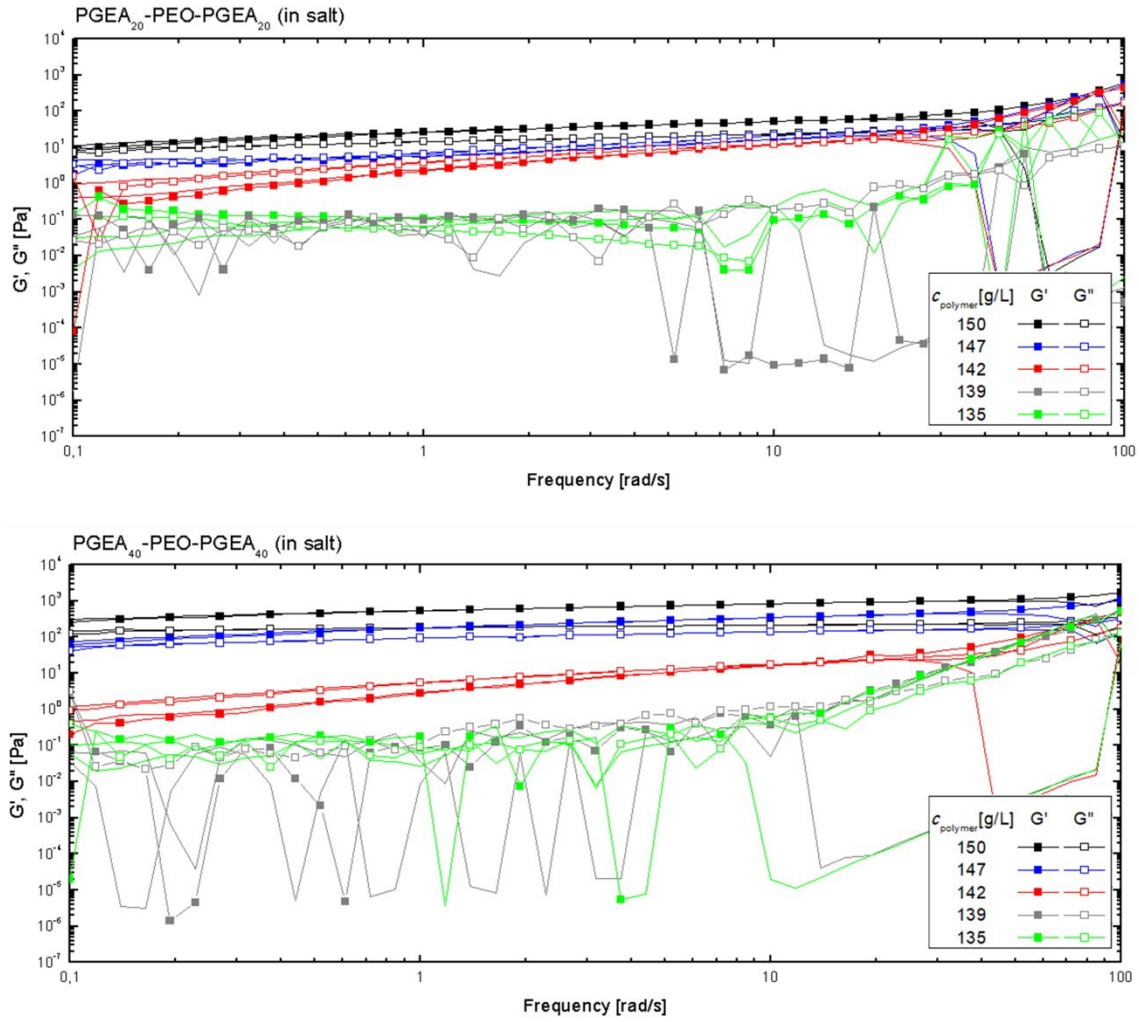

Figure 19: Frequency sweep for PGEA20 and PGEA40 samples at concentrations 150, 147, 142, 139 and 135 g/L in 0.1 M NaCl solution, where G' is storage modulus and G'' is loss modulus. 1. step is represented by line and symbol, 2. step is represented by line.

For storage modulus at frequency 10 Hz (Figure 20 and Figure 21), we see that the decrease of the storage modulus is faster for PGEA20. The length of the PGEA block has impact on the strength of interactions within the PGEA/dodecaborate domains. For samples PGEA20 with concentration 139 g/L in 1. step and for sample PGEA40 with concentration 135 g/L in 2. step, the values of storage modulus are not present in Figure 21 due to the big fluctuations at this frequency.

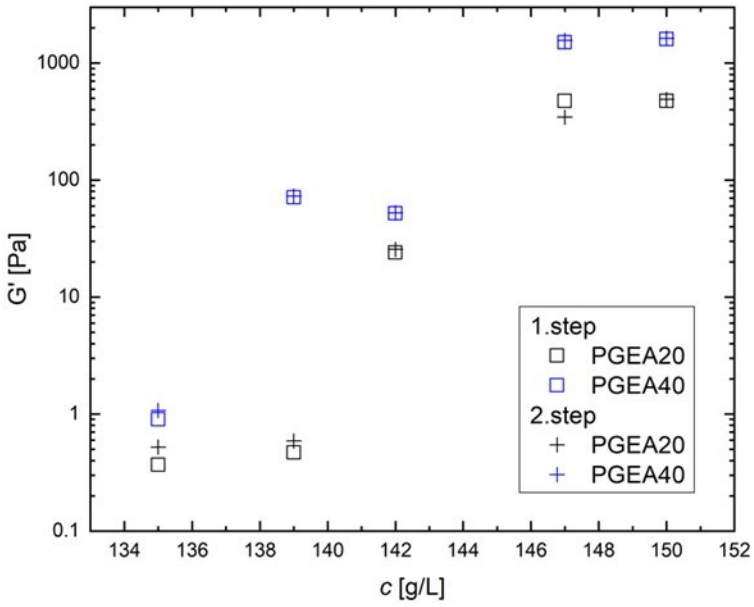

Figure 20: Storage modulus G' for PGEA20 and PGEA40 samples in pure water for different concentrations at frequency 10 Hz; 1. step is frequency sweep from low to high frequencies, 2. step is from high to low frequencies.

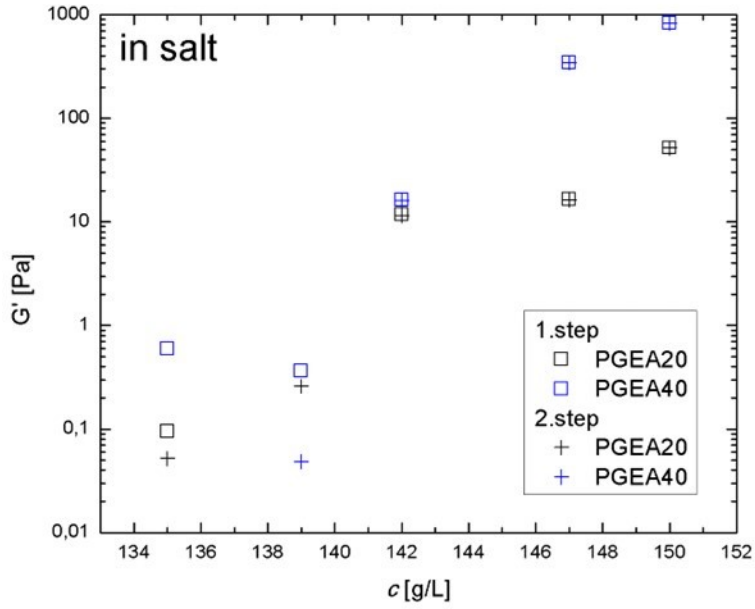

Figure 21: Storage modulus G' for PGEA20 and PGEA40 samples in 0.1 M NaCl solution for different concentrations at frequency 10 Hz; 1. step is frequency sweep from low to high frequencies, 2. step is from high to low frequencies.

Tan(δ), defined as G''/G', for the PGEA20 sample almost does not change with the concentration, except for the region of low frequencies (Figure 22). For the PGEA40 sample, there are more significant differences in values for different concentrations at frequencies over 10 Hz. Samples PGEA40 and PGEA20 (at higher frequencies) have tan(δ) lower than 1, their storage modulus is higher than loss modulus. Decreasing tan(δ) means that the material acts more elastic now, and by applying a load, it has more potential to store the load

rather than dissipating it. Higher values at low frequencies predict self-healing since self-healing happens at stationary state.

The differences in tan(δ) values for different concentrations are more prominent in salt solution (Figure 23). Sample PGEA20 at concentration 150 g/L has tan(δ) lower than 1 (G"<G'), at concentrations 147 and 142 g/L tan(δ) higher than 1 (G">G'), except for higher frequencies. Sample PGEA40 at concentrations 150 and 147 g/L has tan(δ) lower than 1 (G"<G'), at concentration 142 g/L tan(δ) higher than 1 (G">G'), except for higher frequencies. Concentrations 139 and 135 g/L are not shown for either of the samples because of the fluctuation of the data.

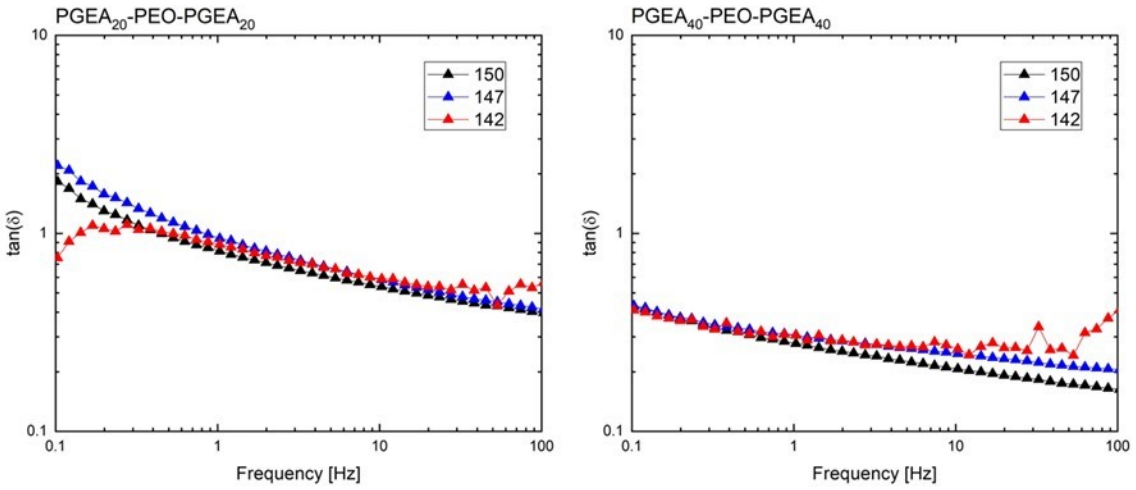

Figure 22: Tan(δ) for PGEA20 and PGEA40 samples at concentrations 150, 147 and 142 g/L in pure water.

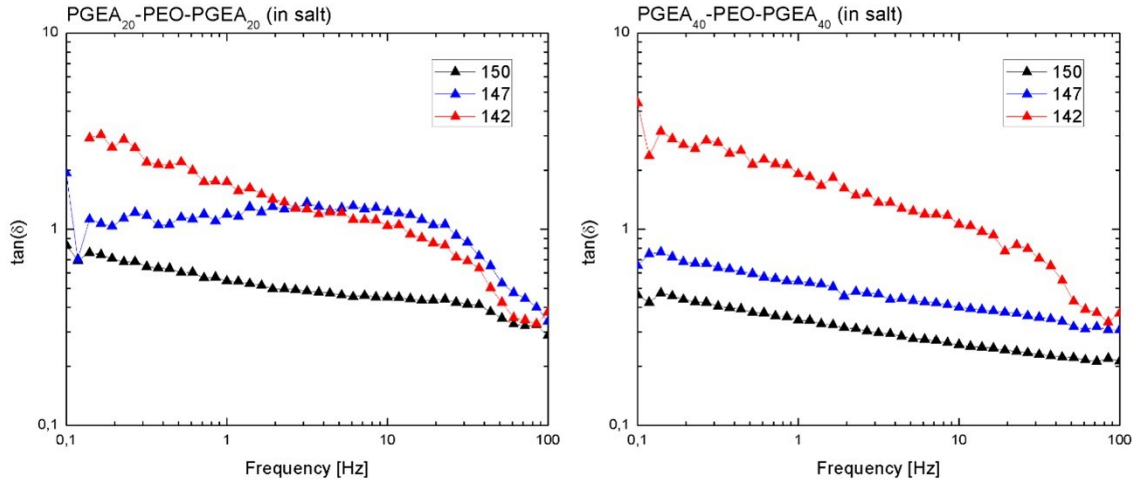

Figure 23: Tan(δ) for PGEA20 and PGEA40 samples at concentrations 150, 147 and 142 g/L in 0.1 M NaCl solution.

By applying shear deformation, we can observer viscosity changes (Figure 24). For both polymers, viscosity drops by several orders of magnitude for concentrations 150, 147 and 142 g/L. For sample PGEA40 with concentration 135 g/L, the viscosity does not change significantly during the measurement. For sample PGEA20 with concentration 139 g/L, the viscosity drops from about 2000 mPa.s to 60 mPa.s. For PGEA40 sample, a shear thinning behaviour is very well observed, PGEA20 displays plateaus at low and high shear rates.

For samples in 0.1 M NaCl solution (Figure 25), the viscosities are lower compared to the samples in pure water. For both polymers, viscosity drops by several orders of magnitude for concentrations 150, 147 for sample PGEA40 and concentration 150 for PGEA20. For other sample PGEA20 the viscosity does not change significantly during the measurement.

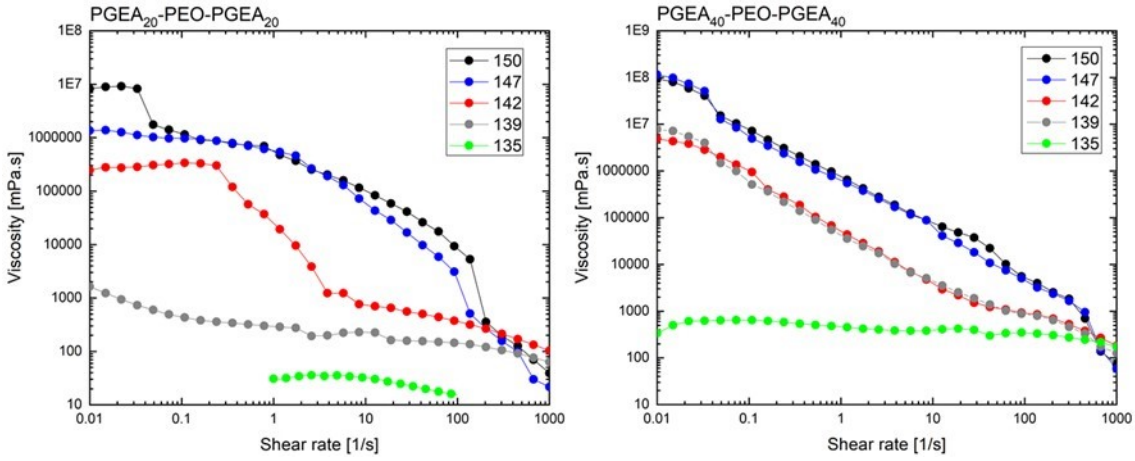

Figure 24: Shear deformation experiment for PGEA20 and PGEA40 samples at concentrations 150, 147, 142, 139 and 135 g/L in pure water.

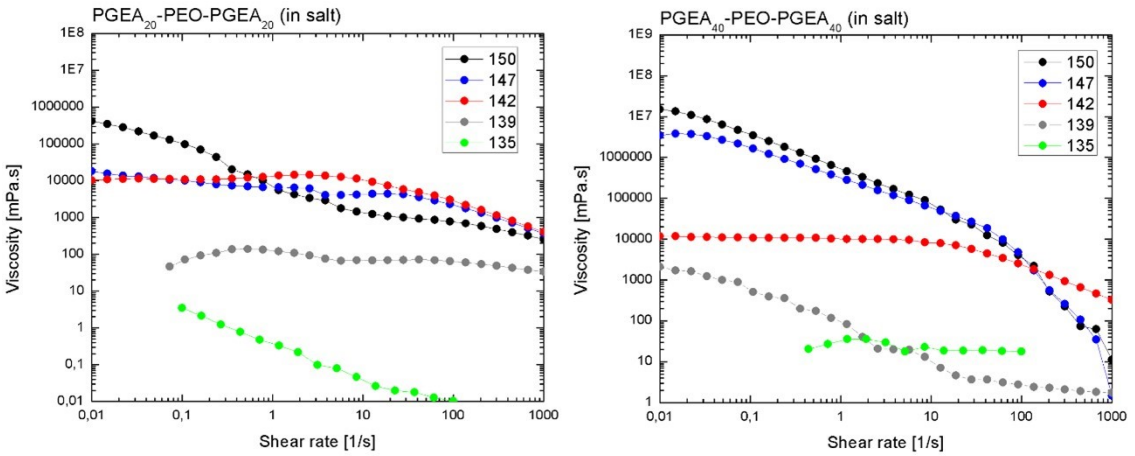

Figure 25: Shear deformation experiment for PGEA20 and PGEA40 samples at concentrations 150, 147, 142, 139 and 135 g/L in 0.1 M NaCl solution.

After applying shear deformation to the sample, a self-healing test (Figure 26) was carried out at oscillation frequency 10 Hz. For all the samples we observe that the values of G' and G" grow during the 30 minutes of the self-healing test. For PGEA40 sample for concentrations 150 and 147 g/L, G' and G" do not reach the values from frequency sweep in 30 minutes. For concentrations 142 and 135 g/L, G' and G" reach the values from frequency sweep. For PGEA20 sample, G' reaches the values from frequency sweep, G" doesn´t reach the values from frequency sweep for concentrations 150, 147 g/L and does reach for concentrations 142, 139 g/L in 30 minutes. G', in many cases, reaches and exceeds values that are higher than values from frequency sweep at 10 Hz, one of possible explanations might be water evaporation from the gel during the experiment.

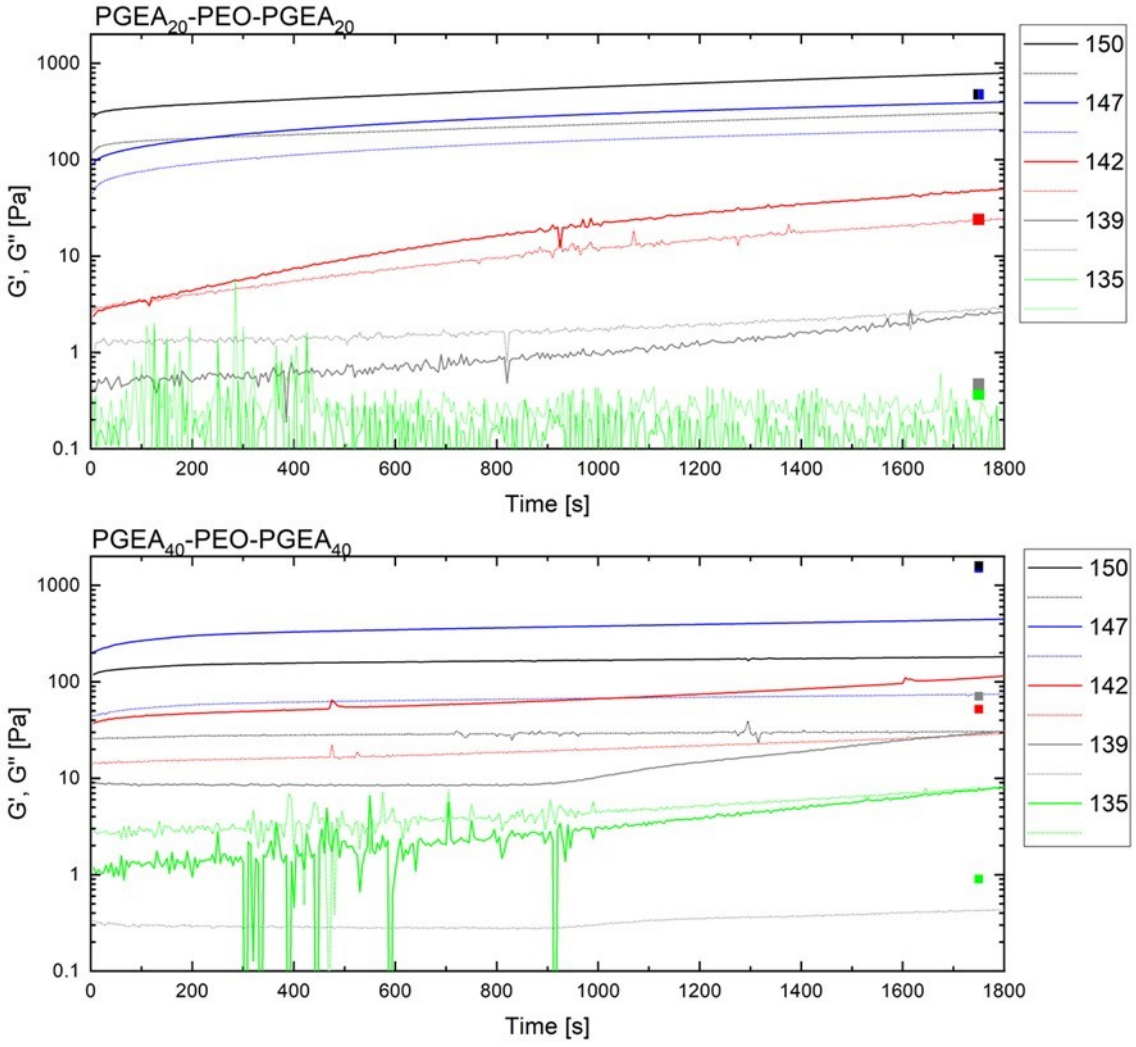

Figure 26: Self-healing test for PGEA20 and PGEA40 samples at concentrations 150, 147, 142, 139 and 135 g/L in pure water, where storage modulus is represented by full lines and loss modulus is represented by dotted lines. Full squares represent storage modulus obtained from frequency sweep at frequency 10 Hz.

In 0.1 M NaCl solution (Figure 27), all samples PGEA20 and PGEA40 at concentrations 142, 139 and 135 g/L show almost no increase in values of storage and loss modulus over the course of the 30-minute self-healing test. These samples did not reach high values of storage and loss modulus in frequency sweep and the shear deformation that was put on them prior to self-healing test might not have been enough to break the gel network. Samples with concentrations 150 and 147 g/L show increase of storage and loss moduli but do not reach the values from frequency sweep at 10 Hz.

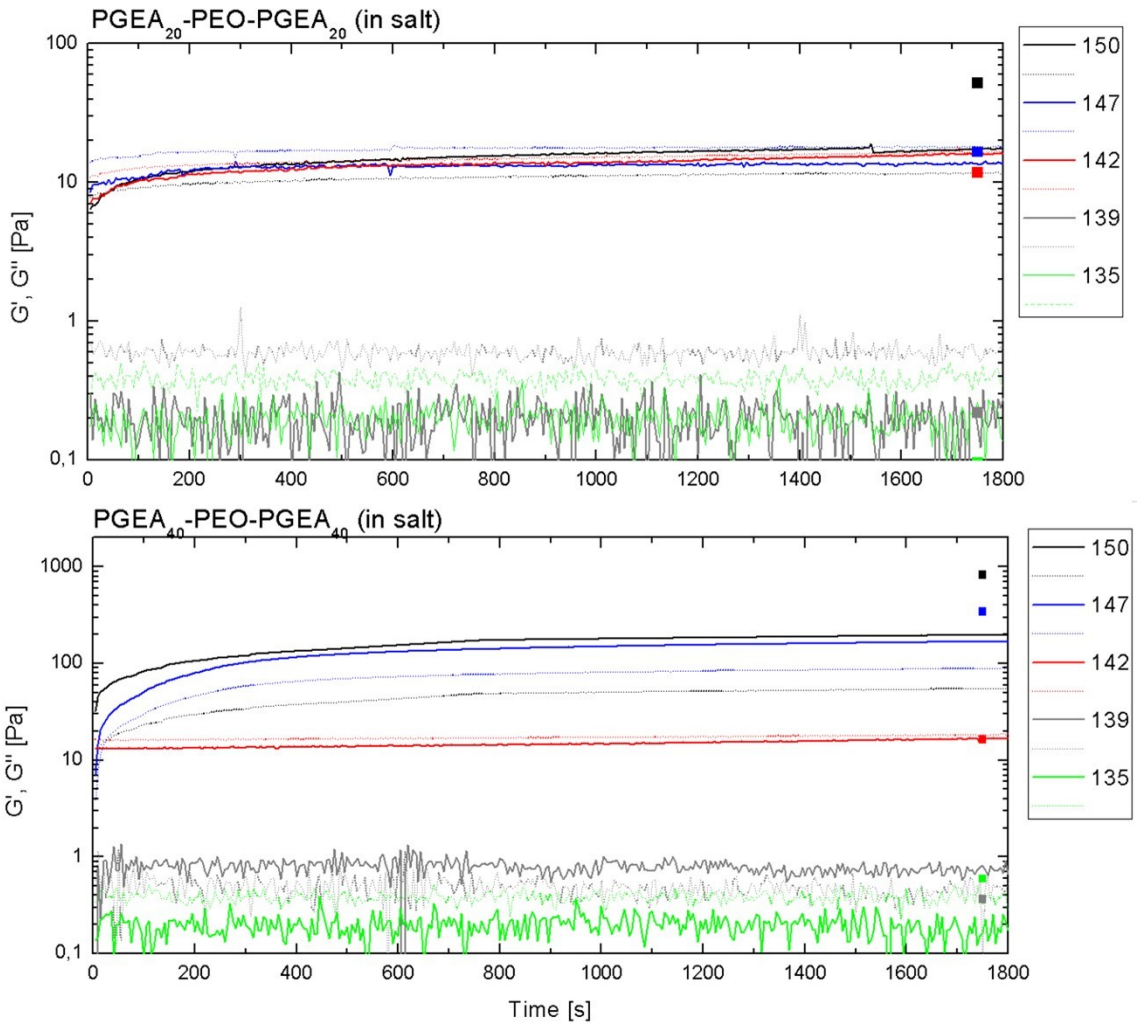

Figure 27: Self-healing test for PGEA20 and PGEA40 samples at concentrations 150, 147, 142, 139 and 135 g/L in 0.1 NaCl solution, where storage modulus is represented by full lines and loss modulus is represented by dotted lines. Full squares represent storage modulus obtained from frequency sweep at frequency 10 Hz.

Rheology measurements show that the length of the PGEA block, which forms domains due to the guanidinium-dodecaborate interactions in hydrogels, has significant impact on its mechanical properties. Gels with longer PGEA blocks (40 units) are stronger than gels with shorter PGEA blocks (20 units). In salt solution (0.1 M NaCl), gels of the same polymer are

weaker compared to gels in pure water. All the gels exhibit shear-thinning behaviour both in pure water and in 0.1 M NaCl.

6.1.3. Fluorescence spectroscopy

For both polymer samples, $PGEA_{20}$-PEO-$PGEA_{20}$ and $PGEA_{40}$-PEO-$PGEA_{40}$, 50 mg of polymer was dissolved in 500 μL of water and 25 μL of 1 g/L stock solution of fluorescent probe (FBC, Figure 12) was added. Afterwards, dodecaborate was added according to theoretical electroneutral value of guanidinium-to-dodecaborate ratio of 0.5 (Table 3). Samples were left to equilibrate for 1 day before starting the measurement.

Table 3: Sample preparation for time resolved anisotropy and their visual description for concentration 100 g/L, where w % (P+B12) is weight percentage of polymer and dodecaborate in sample, m(P) is weight of the polymer and m(B12) is weight of the dodecaborate.

PGEA m	***w* % (P+B_{12})**	***m*(P) [mg]**	***m*(B_{12}) [mg]**	**visual description *c* = 100 g/L**
20	10.50	50	8.63	viscous solution
40	10.93	50	11.21	viscous solution

Before sample measurement a correction measurement, G-factor, was done since detectors and monochromators may be biased for one plane of polarization. The value of G-factor that was measured and used in all experiments was 0.885. Time resolved anisotropy measurements were done in pure water at 25 and 60 °C, and in 0.1 M NaCl solution at 25 °C. We can see on the anisotropy curves (Figure 28, Figure 29) that there is significant residual anisotropy, probably caused by immobilization of the fluorescent probes by interaction with cationic blocks. Anisotropy is also influenced by both increasing the temperature and presence of salt. The anisotropy decay for both samples show non-zero limiting anisotropy, r_∞, since fluorophore is immobilized and not fully free to rotate. The anisotropy decay shows a fast mode which represents the free fluorescent probe in sample and a slow mode that represents the fluorescent probe in PGEA/dodecaborate domains. By fitting the anisotropy decay using reconvolution and correction by G-factor were obtained fluorescence anisotropy and anisotropy decay times summarized in Table 4 and Table 5 for all measurements. The quality of the fit was judged by χ^2 values, which are low for all samples.

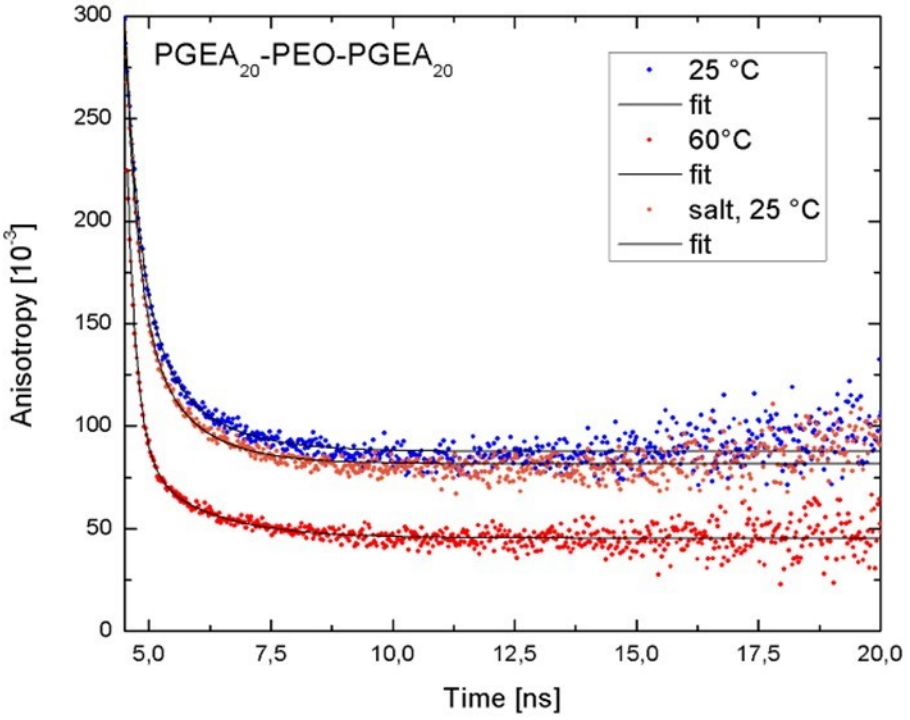

Figure 28: Time resolved anisotropy curves for PGEA20 sample at 25 and 60 °C in pure water and at 25 °C in 0.1 M NaCl solution with corresponding fits.

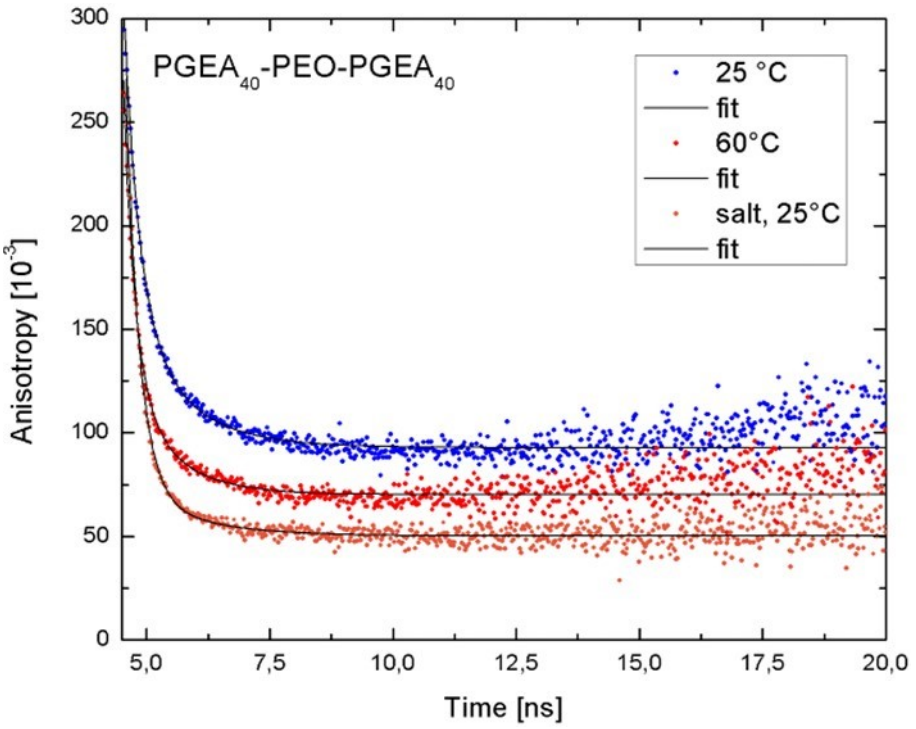

Figure 29: Time resolved anisotropy curves for PGEA40 sample at 25 and 60 °C in water and at 25 °C in 0.1 M NaCl with corresponding fits.

Table 4: Fluorescence anisotropy r, anisotropy decay times ϕ and residual anisotropy r_∞, for samples $PGEA_{20}$-PEO-$PGEA_{20}$/dodecaborate in pure water at 25 and 60 °C and in 0.1 M NaCl solution at 25 °C.

Parameter	25 °C	60 °C	salt, 25 °C
r_1	0.1416 ± 0.0034	0.1388 ± 0.0011	0.1496 ± 0.0080
ϕ_1 [ns]	0.302 ± 0.012	0.2023 ± 0.0044	0.276 ± 0.015
r_2	0.0815 ± 0.0032	0.0411 ± 0.0018	0.0783 ± 0.00668
ϕ_2 [ns]	1.123 ± 0.040	1.391 ± 0.089	1.042 ± 0.072
r_∞	0.0877 ± 0.0004	0.0454 ± 0.0003	0.0817 ± 0.0003
χ^2	1.8530	1.1250	1.1450

Table 5: Fluorescence anisotropy r, anisotropy decay times ϕ and residual anisotropy r_∞, for samples $PGEA_{40}$-PEO-$PGEA_{40}$/dodecaborate in pure water at 25 and 60 °C and in 0.1 M NaCl solution at 25 °C.

Parameter	25 °C	60 °C	salt, 25 °C
r_1	0.145 ± 0.0084	0.1429 ± 0.0034	0.1960 ± 0.0045
ϕ_1 [ns]	0.31 ± 0.018	0.2309 ± 0.0060	0.2750 ± 0.0036
r_2	0.0708 ± 0.0090	0.0575 ± 0.0031	0.0244 ± 0.0021
ϕ_2 [ns]	1.086 ± 0.048	0.913 ± 0.048	1.285 ± 0.098
r_∞	0.0929 ± 0.0006	0.0702 ± 0.0006	0.0502 ± 0.0003
χ^2	1.6350	1.2730	1.0360

6.1.4. SAXS

For both polymer samples, $PGEA_{20}$-PEO-$PGEA_{20}$ and $PGEA_{40}$-PEO-$PGEA_{40}$, 30 mg of polymer was dissolved in 200 µl of pure water and dodecaborate was added according to theoretical electroneutral value of guanidinium/dodecaborate ratio of 0.5. (Table 6). Samples were left to equilibrate for 1 day before starting the measurement.

Table 6: Sample preparation for SAXS, WAXS and their visual description, where c(P) is concentration of polymer, w % (P+B12) is weight percentage of polymer and dodecaborate in sample, m(P) is weight of the polymer and m(B12) is weight of the dodecaborate.

PGEA m	*c* (P) [g/L]	*w* % (P+B_{12})	*m*(P) [mg]	*m*(B_{12}) [mg]	visual description
20	150	14.98	30	5.21	gel
	140	14.16	30	4.83	honey
	1	0.11	1	0.17	solution
40	150	15.51	30	6.71	gel
	130	13.77	30	5.83	honey
	1	0.11	1	0.22	solution

Figure 30 and Figure 31 show SAXS profile for samples PGEA20 and PGEA40 respectively after subtraction of the background. SAXS peak are seen for samples PGEA20 for concentrations 150 and 140 g/L and for PGEA40 for concentration 150 g/L at similar *q* values of approximately 0.03 $Å^{-1}$. The preliminary fitting of the experimental curves provided the size of the nanodomains and their distance within the studied gels (listed in Table 7). The PGEA-dodecaborate domains are probably bigger in the samples with longer PGEA blocks. It is also evident, that the gel dilution caused structural changes. Detailed SAXS and cryoTEM studies are planned in the future research.

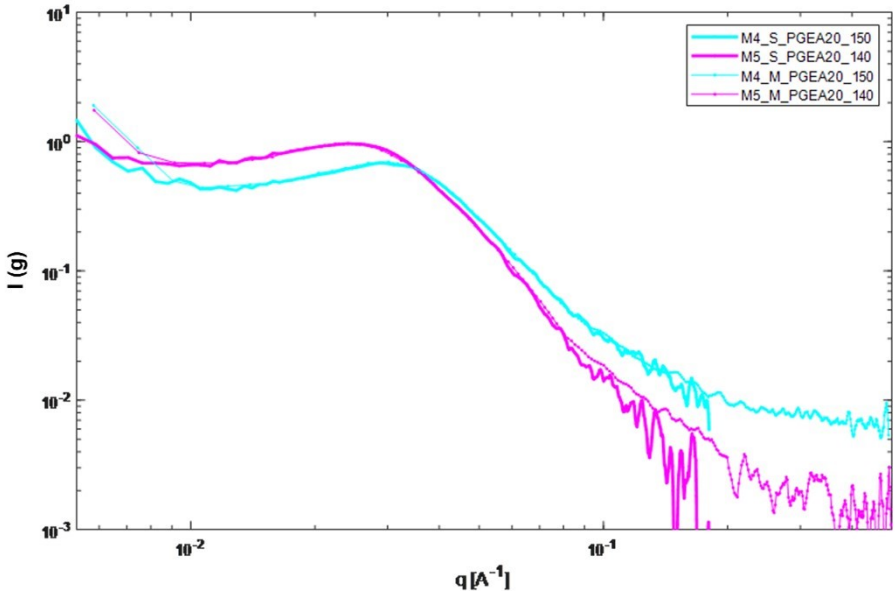

Figure 30: Scattering intensity vs. scattering vector q, for samples PGEA20.

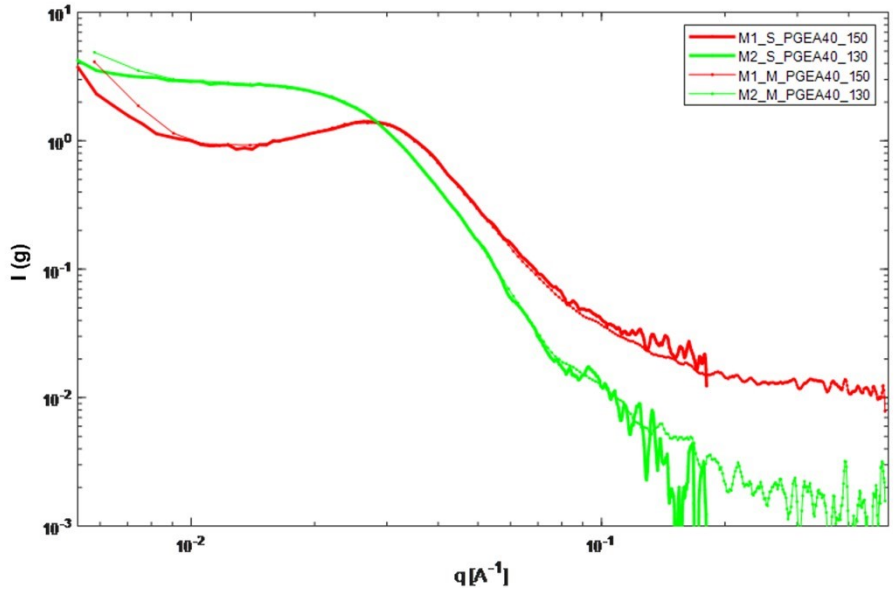

Figure 31: Scattering intensity vs. scattering vector q, for samples PGEA40.

Table 7: Parameters from SAXS measurements for both PGEA-PEO-PGEA polymers, where c(P) is concentration of polymer, R_g and I_0 are gyration radius and scattering intensity at q=0 of the nanoparticles, R_{gC} and I_{0C} are gyration radius and scattering intensity at q=0 of the particle core, R_{1m} is radius of the particle from the first minimum and DB is Bragg distance.

PGEA m	*c*(P) [g/L]	R_g [Å]	I_0	R_{1m} [Å]	DB [Å]	R_{gC} [Å]	I_{0C}
20	150	290	3.0	430	200	43	1.3
	140	200	1.5	462	240	51	1.7
40	150	290	7.6	382	220	54	3.0
	130	240	7.0	512	280	64	4.0

6.2. PNIPAM-PAA-PNIPAM

Triblock copolymers PNIPAM-PAA-PNIPAM, with different PNIPAM block lengths, 25 and 50 units, respectively, and with the length of the PAA block 100 units were synthesized. Interactions of PNIPAM block of these copolymers with cobalt bis(dicarbollide) (COSAN) in aqueous solutions were studied. Gels can be formed at high polymer concentrations after addition of COSAN to polymer solution. To check the individual steps of the synthesis and for determination of molar mass nuclear magnetic resonance and size exclusion chromatography were used. Thermoresponsive properties of prepared copolymers and their gels with COSAN were investigated by dynamic light scattering and rheological measurements at TU Berlin in the laboratory of Prof. M. Gradzielski. In this chapter PNIPAM25 refers to $PNIPAM_{25}$-PAA-$PNIPAM_{25}$/COSAN and PNIPAM50 refers to $PNIPAM_{50}$-PAA-$PNIPAM_{50}$/COSAN.

6.2.1. Synthesis

Different PNIPAM-PAA-PNIPAM triblock copolymers with varying thermoresponsive PNIPAM block lengths were synthesized via RAFT polymerization in three steps (Figure 32). In first step, AIBN, CTA, NIPAM monomer were weighted into a small round bottom flask, and then solvent-dioxane was added. This was purged under nitrogen for 10 minutes. Afterwards, the solution was bubbled with nitrogen for 40 minutes. Next, the mixture was stirred for 1 hour at 80 °C, and after that it was cooled down in ice bath. Polymers were precipitated in cold ether. In second step, AIBN, PNIPAM polymer prepared in previous step, and *tert*-butyl acrylate monomer were weighted into a small round bottom flask, and then solvent-dioxane was added. This was purged under nitrogen for 10 minutes. Afterwards, the solution was bubbled with nitrogen for 40 minutes. Next, the mixture was stirred for 1 hour at 80 °C, and after that it was cooled down in ice bath. Polymers were precipitated in water/MeOH – 10/1 or cold ether depending on the length of the PNIPAM and PtBA block. In the third step, PNIPAM-PtBA-PNIPAM copolymer was weighted into a small round bottom flask, then dissolved in dry DCM, and after it was fully dissolved TFA was added. The mixture was stirred for 48 hours at 25 °C. Afterwards, the precipitant was washed with DCM and the rest of the solvent was evaporated. Solid was dispersed in water and freeze dried. The result was white powder.

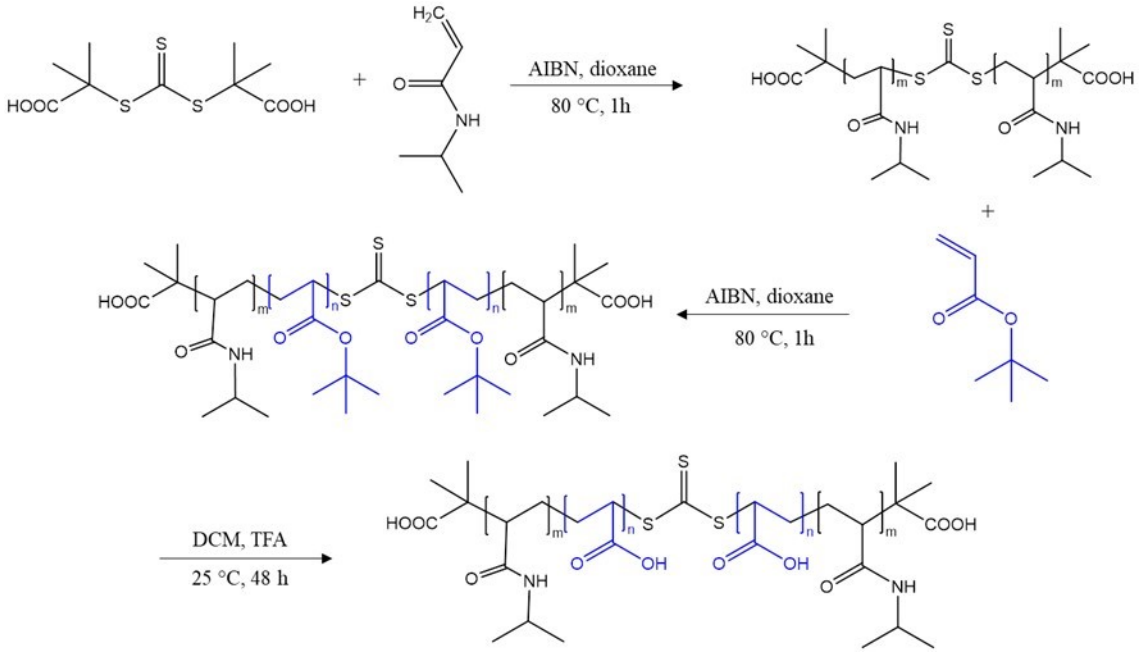

Figure 32: Synthetic route for RAFT polymerization of PNIPAM-PAA-PNIPAM.

6.2.2. NMR

To confirm successful polymerization after each step of the synthesis, ^{1}H NMR spectroscopy was used. For PNIPAM polymers and PNIPAM-PtBA-PNIPAM copolymers chloroform-d ($CDCl_3$) was used as solvent, for PNIPAM-PAA-PNIPAM deuterium oxide (D_2O) was used as a solvent. In Figure 33, there are shown ^{1}H NMR spectra for synthesis of $PNIPAM_{25}$-PAA_{100}-$PNIPAM_{25}$, copolymer with 50 segments in PNIPAM block shows similar spectra. ^{1}H NMR spectroscopy was used to check kinetics of the polymerization.

After polymerization of PNIPAM (top spectrum in Figure 33), a small amount of sample was taken from the reaction flask and $CDCl_3$ was added. At ppm 1.1, we see CH_3 signal and at ppm around 4 we see CH signal that belong to the isopropyl group of PNIPAM. The broad signals in the ppm range from 1.3 to 2.3 belong to the polymer backbone. Signal at ppm 5.8 belongs to the hydrogen of NH group of PNIPAM. In the spectrum, there is prominent signal of dioxane and we can also see signals of the NIPAM monomer, since the sample was taken straight from the reaction flask. The polymer is rid of the monomer residues after precipitation in cold ether.

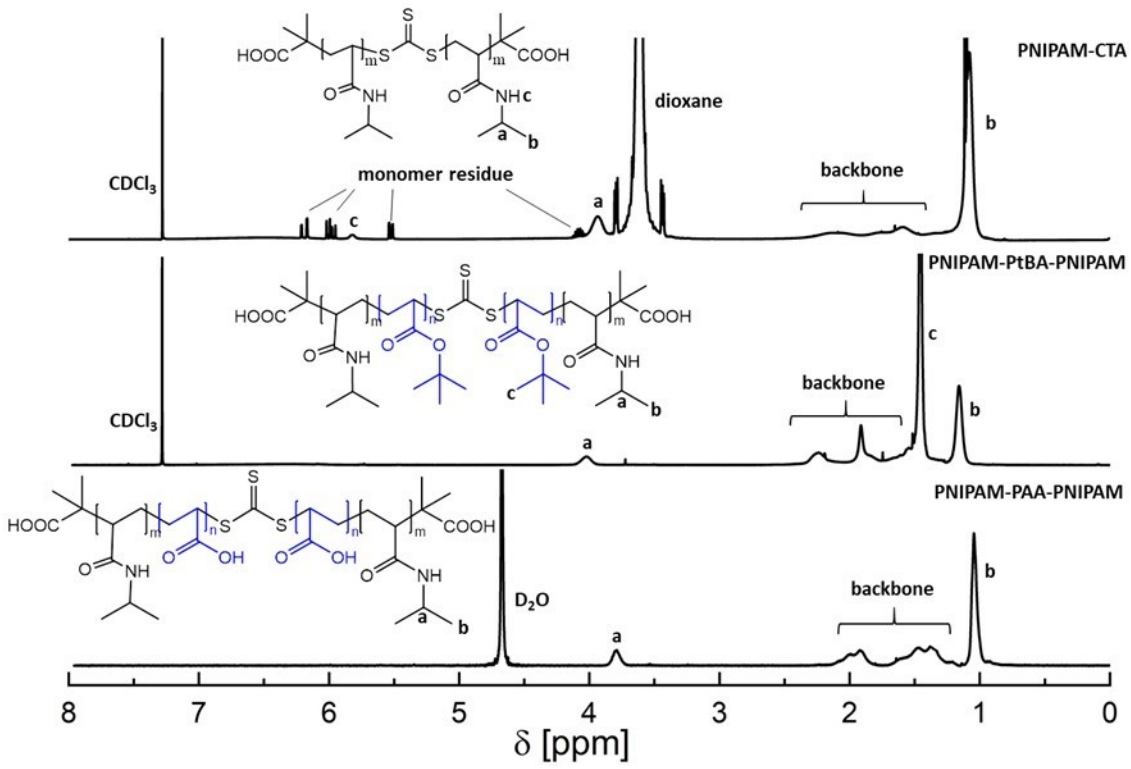

Figure 33: [1]H NMR spectra for individual steps of the polymerization. Signal assignments are shown in the structures. As solvent was used chloroform-d ($CDCl_3$) or deuterium oxide (D_2O).

After copolymerization with *tert*-butyl acrylate (middle spectrum in Figure 33), 5 mg of dry product was dissolved in 800 µl of $CDCl_3$. We observe new CH_3 signal at ppm 1.4 that belongs to the *tert*-butyl group of PtBA. Signals at 1.1 and 4 ppm belong to the PNIPAM block and broad signals at low ppm belong to the polymer backbone.

After the hydrolysis of the copolymer (bottom spectrum in Figure 33), 5 mg of dry product was dissolved in 800 µl of D_2O. The hydrolysis was confirmed by absence of the CH_3 signal of *tert*-butyl group. Again, peaks at 1.1 and 4 ppm belong to the isopropyl group of PNIPAM and broad peaks at low ppm belong to the polymer backbone.

Kinetics of the RAFT polymerization was checked by ^{1}H NMR spectroscopy, to determine the point when the conversion is around 60-70% to achieve narrow polymer dispersity. Sample was taken from the reaction flask using cannula. For kinetics measurements (Figure 34) of polymerization of NIPAM, times 10, 20, 40, 60, 90, 120 and 180 minutes were chosen. At time 60 minutes, the conversion was around 85 %. For the second step of RAFT polymerization times 10, 20, 40, 60, 90, 120, 150, 180, 210 and 240 were chosen. At time 60 minutes conversion was about 75 %.

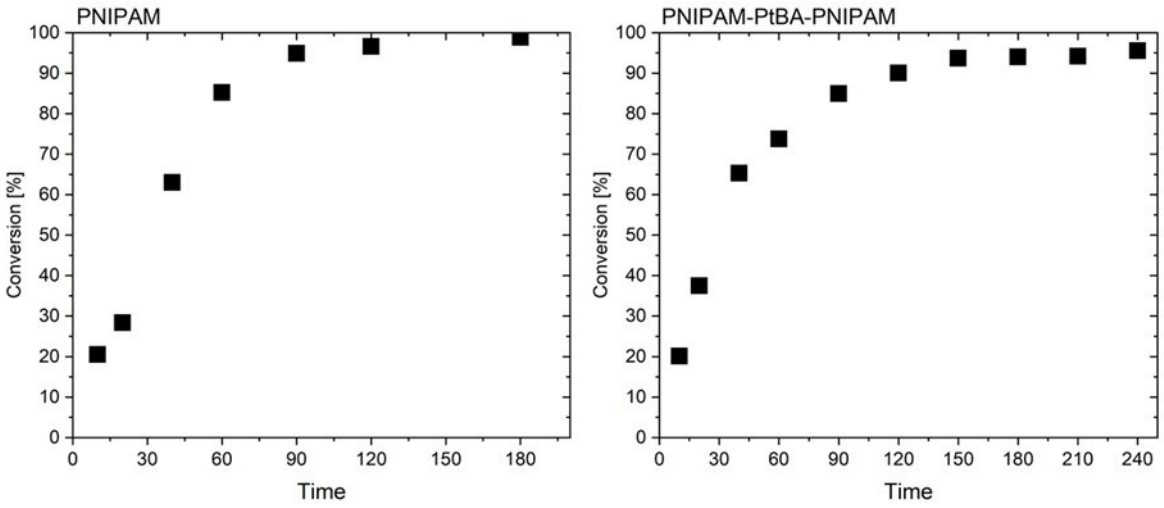

Figure 34: Kinetics measurements done by ^{1}H NMR for polymerization of NIPAM and copolymerization of PNIPAM with tert-butyl acrylate.

6.2.3. SEC

The molecular weight and dispersity of PNIPAM polymers and PNIPAM-PtBA-PNIPAM copolymers were characterized by size exclusion chromatography (SEC). Into a small vial, 5 mg of polymer was weighted and dissolved in 1 ml of DMA. Sample was then filtrated through PTFE filter into a small vial with septum. SEC traces, in Figure 35 and Figure 36 show molecular weight distribution of polymers. The shift of the peak to the lower retention time shows successful copolymerization, it was confirmed also by ^{1}H NMR (see Section 6.2.2). PNIPAM-CTA-PNIPAM samples (black in Figure 35 and Figure 36, labelled as N-CTA-N) generally exhibit low dispersity ($Đ$<1.20) and monomodal size distribution (Table 8). PNIPAM-PtBA-PNIPAM samples (blue in Figure 35, Figure 36 labelled as N-B-N) all exhibit dispersity over than 1.20 and show high intensity mode at retention time about 20 minutes. The number-average molar mass and dispersity of the polymers are summarized in Table 8.

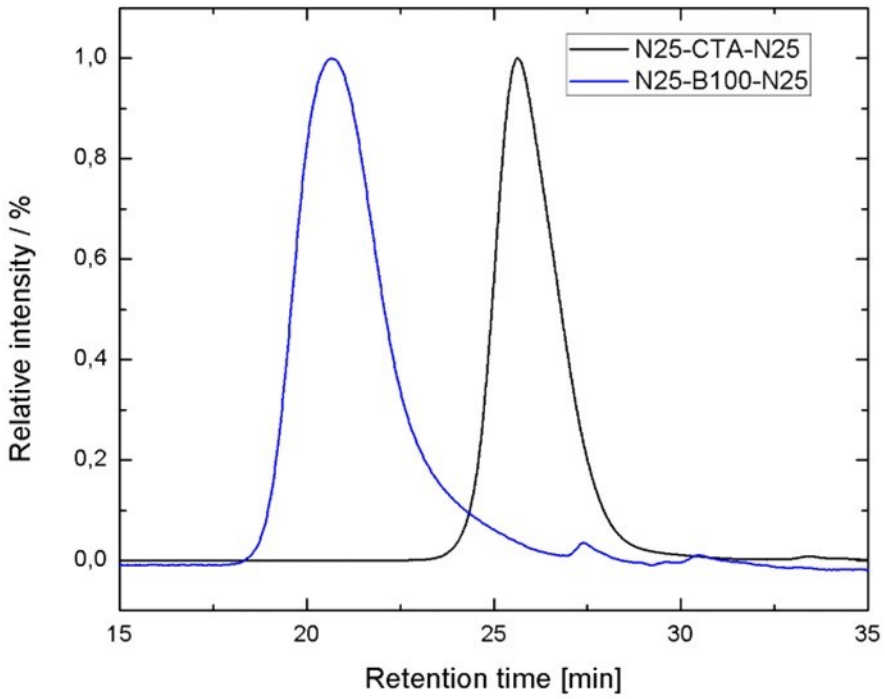

Figure 35: SEC traces of PNIPAM$_{25}$-CTA-PNIPAM$_{25}$(black) and PNIPAM$_{25}$-PtBA$_{100}$-PNIPAM$_{25}$ (blue).

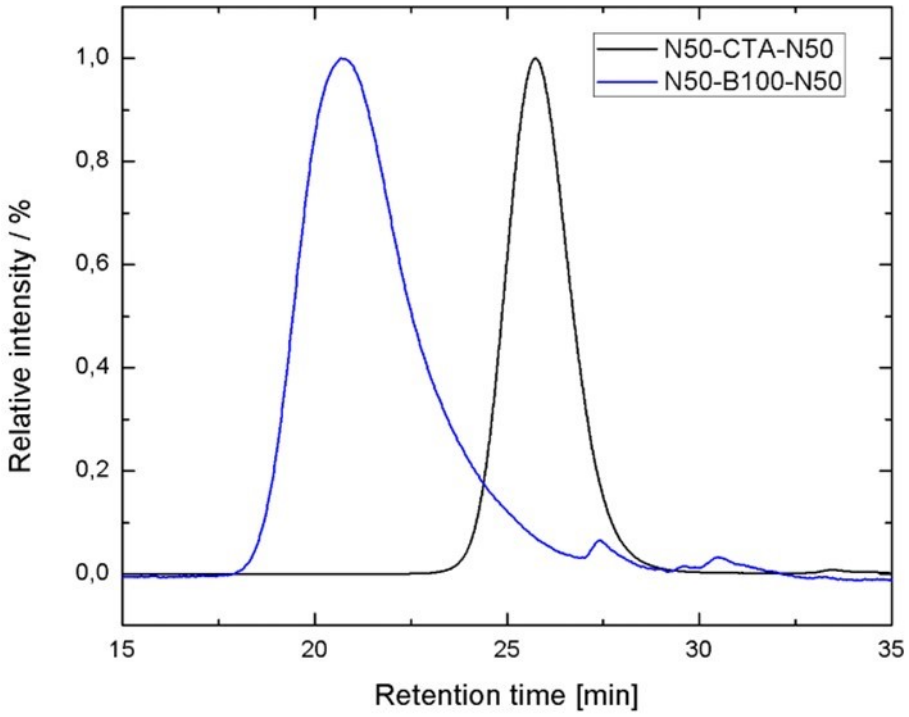

Figure 36: SEC traces of PNIPAM$_{50}$-CTA-PNIPAM$_{50}$ (black) and PNIPAM$_{50}$-PtBA$_{100}$-PNIPAM$_{50}$ (blue).

Table 8: Summary of molecular weight $M_{n,\,SEC}$ and dispersity Đ data from SEC. Conversion of the reaction was obtained by ^1H NMR.

Sample	conversion (%)	$M_{n,\,SEC}$ [kg/mol]	$Đ_{SEC}$
PNIPAM25-CTA-PNIPAM25	65	8.9	1.09
PNIPAM50-CTA-PNIPAM50	65	16.7	1.16
PNIPAM25-PtBA100-PNIPAM25	70	18.6	1.29
PNIPAM50-PtBA100-PNIPAM50	61	28.3	1.24

6.2.4. DLS

For preliminary DLS measurements, 5 mg of PNIPAM-PAA-PNIPAM copolymer was dissolved in 1 ml of pure water. Two kinds of samples were prepared, ones containing only a polymer in water and others with COSAN (molar ratio of COSAN to PNIPAM blocks was 1:10) as well. Samples were left to equilibrate for 1 day before starting the measurement. Shown in Figure 37, there are autocorrelation functions at 90° for polymer at concentration 5 g/L with and without COSAN, which should act as gelation agent due to PNIPAM/COSAN interaction, while PAA blocks do not interact with COSAN. For the triblock copolymer sample without added COSAN, we assumed gelation upon heating, because PNIPAM blocks should collapse (LCST behaviour), and form compact domains interconnected by swelled PAA blocks. Even though DLS experiments showed thermoresponsivity, no gels but several types of nanaoparticles were observed. Nanogels were probably formed for these samples. The DLS experiments revealed that both PNIPAM block length and presence of COSAN have impact on size of the nanogels and thermoresponsive behaviour of the systems.

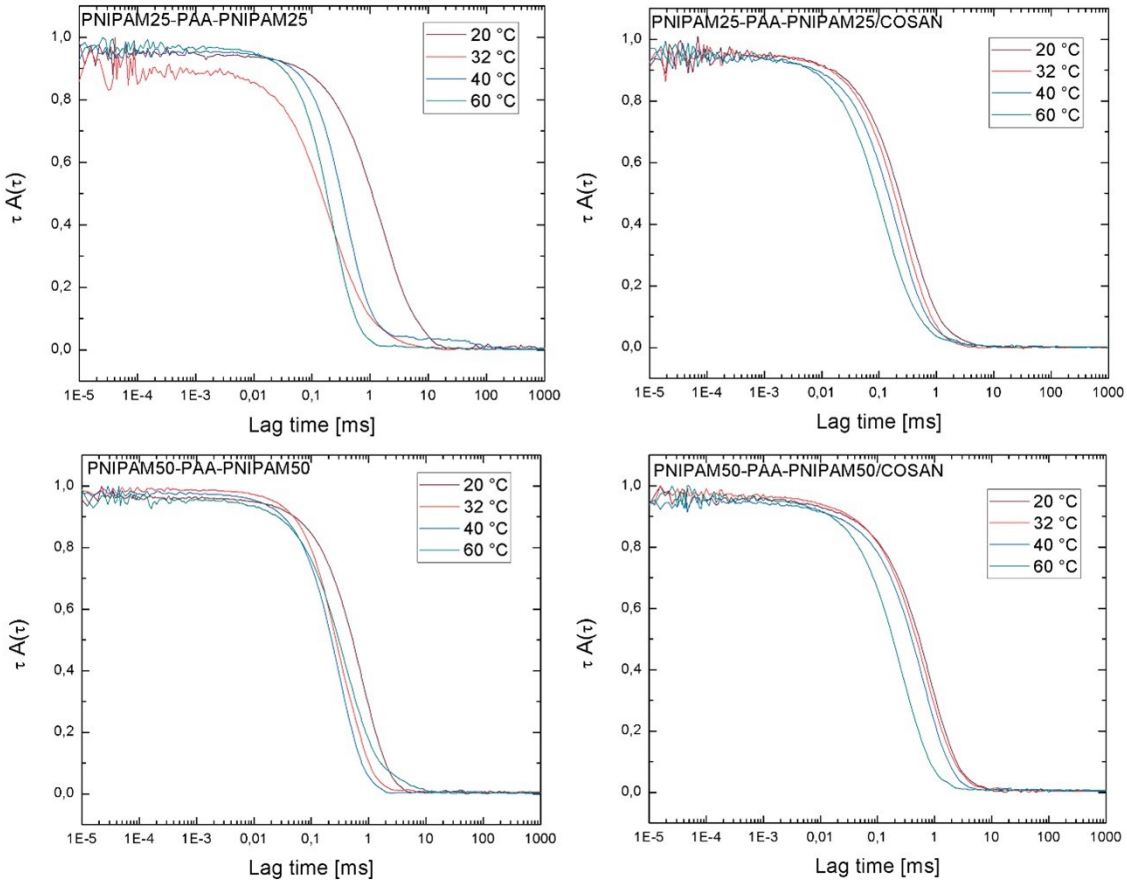

Figure 37: Normalized autocorrelation function of polymer systems PNIPAM$_{25}$-PAA-PNIPAM$_{25}$ and PNIPAM$_{50}$-PAA-PNIPAM$_{50}$ with and without COSAN; polymer concentration was 5 g/L.

6.2.5. Rheology

For both polymers, PNIPAM$_{25}$-PAA-PNIPAM$_{25}$ and PNIPAM$_{50}$-PAA-PNIPAM$_{50}$, samples were prepared with polymer concentration 100 g/L, and molar ratio of COSAN to PNIPAM blocks was 1:10 (photograph of sample in Figure 38). The samples without COSAN produced undefined precipitants at high polymer concentrations and were not used in following studies.

Amplitude sweep and frequency sweep of the polymer/COSAN gels (PNIPAM25 and PNIPAM50 samples) were performed at temperatures 20, 32, 36 and 40 °C. To avoid water evaporation due to higher temperatures, around the bottom geometry was added distilled water.

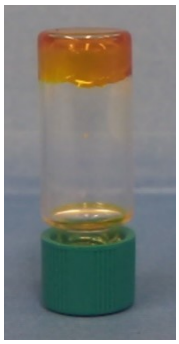

Figure 38: Photograph of PNIPAM25 sample used for rheology measurements.

An amplitude sweep (Figure 39) was carried out first to determine linear viscoelastic region. Full squares represent G', empty ones G". For all samples, G' is higher than G". With the increasing temperature, values of G' also increase, this increase is more prominent in sample PNIPAM25. Both samples have higher storage modulus than loss modulus at all temperatures, they are more solid-like. Sample PNIPAM25 has higher storage modulus compared to sample PNIPAM50, sample PNIPAM25 forms stronger gels.

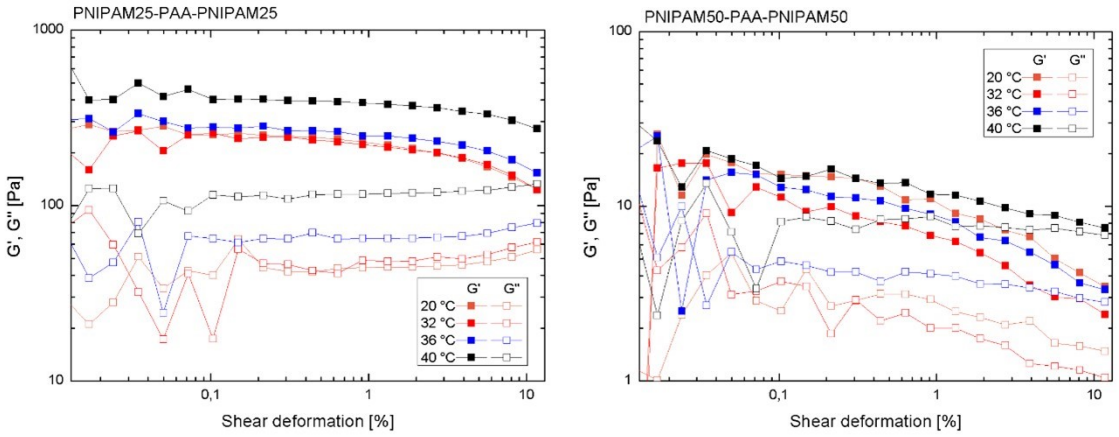

Figure 39: Amplitude sweep for PNIPAM25 and PNIPAM50 samples at temperatures 20, 32, 36 and 40 °C, where G' is storage modulus and G" is loss modulus.

Frequency sweep (Figure 40) was carried out at 1% strain. Full squares represent G', empty ones G". In the first step, the frequency goes from low values to high values in the second step it goes from high values to low values. With the increasing temperature was observed increase in values of G' for both polymer samples. The values for both samples significantly differed at temperatures 20 and 32 °C. Further, the increase at temperatures 36 and 40 °C is more prominent for sample PNIPAM25.

In Figure 41, is shown plot of storage modulus from frequency sweep at frequency 10 Hz plotted against temperature. The sample PNIPAM50 displays the temperature response faster than sample PNIPAM25.

Rheology measurements show that the samples with longer PNIPAM blocks form weaker gels with COSAN. Both samples show temperature response, that is shifted to higher temperature than 32 °C (LCST of pure PNIPAM in water).

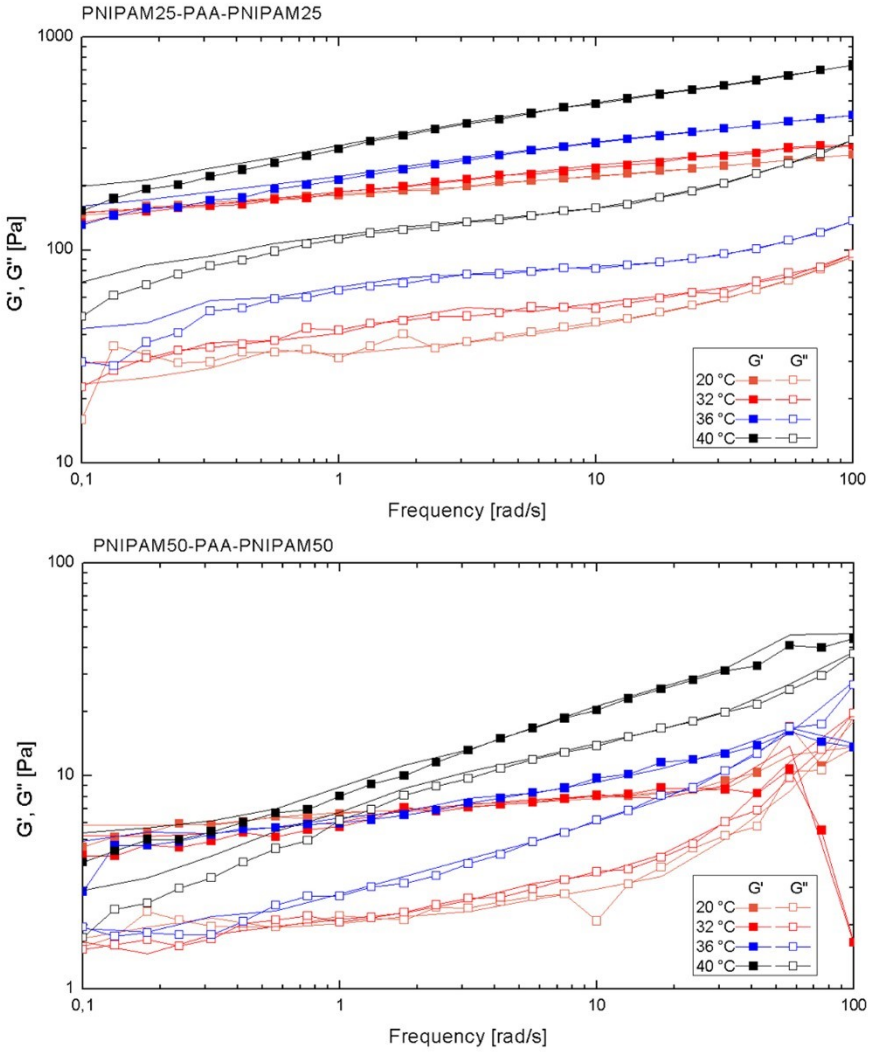

Figure 40: Frequency sweep for PNIPAM25 and *PNIPAM*50 samples *at temperatures 20, 32, 36 and 40 °C, where G' is storage modulus and G'' is loss modulus. 1. step is represented by line and symbol, 2. step is represented by line.*

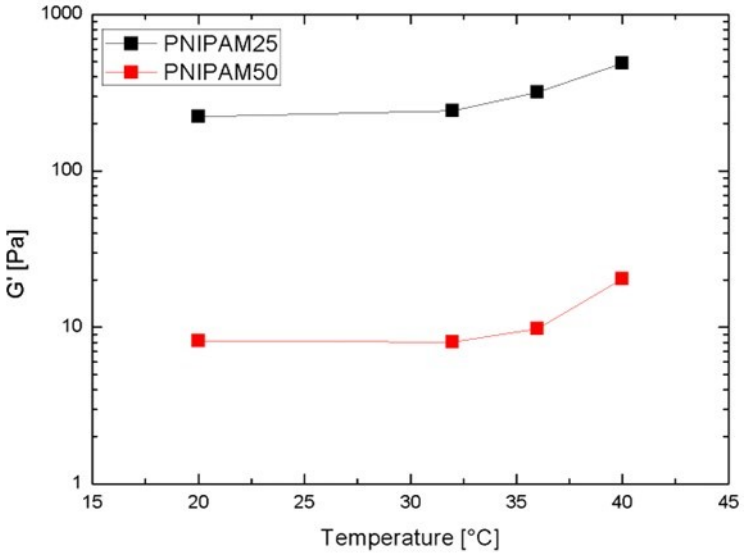

Figure 41: Values of storage modulus plotted against temperature for PNIPAM25 sample (black) and PNIPAM50 sample (red).

6.3. PEO/COSAN

PEO/COSAN forms insoluble complex in aqueous solutions and the precipitation is induced by salt presence.[7,9,59] The influence of the counter ion of lithium and sodium salts on the PEO/COSAN complex formation was studied. One of the decisive contributions is the formation of dihydrogen bonds between hydrogen atoms attached to boron atoms and hydrogen atoms in repeating PEO units. It is also important that alkaline cations interact with oxygen atoms of PEO.[7,9,59] Salts chosen for the study were MF, MCl, MI, MSCN and M_2SO_4 (M is lithium and sodium). We can also compare an influence of lithium and sodium cation. The results from this study will be used for design of stimuli-responsive gels and nanoparticles based on PEO/COSAN interaction.

6.3.1. Sample preparation

Na[COSAN] and Li[COSAN] were prepared by cation exchange described in Section 5.1. The purity of M[COSAN] was checked by ^{1}H NMR spectroscopy in D_2O (Figure 42). Both lithium and sodium COSAN show sharp peak at ppm around 3.9 that belongs to the CH group and broad peak in the ppm range from 1 to 3.5 that belong to the BH groups of the cluster.

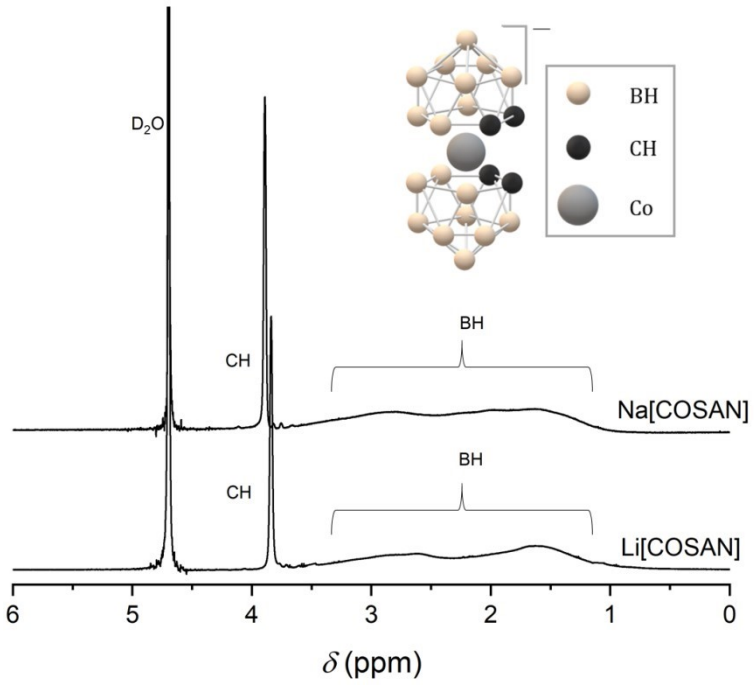

Figure 42: ^{1}H NMR spectra of Li[COSAN] and Na[COSAN]. Signal are assigned accordingly with the model presented.

Into a small vial 2 mg of PEO with M_n = 20 kg/mol was weighted and polymer was dissolved in pure water. Next, COSAN solution was added in ratio of 1 COSAN cluster to 10 PEO segments (Ref. 9). Lastly, into respective vials, five different lithium or sodium salts were added to get 0.1 M salt solution (Figure 43). Final volume of the samples was 1.5 ml.

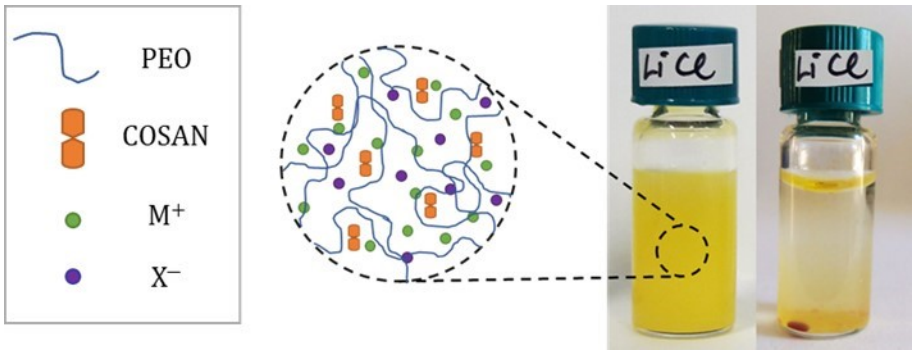

Figure 43: Schematic of the system in the sample. The sample is depicted just after preparation (left) and after formation of the PEO/COSAN precipitant on the bottom in 3 months (right). M is either Li or Na and X is F, Cl, I, SCN or SO_4; On the photograph, PEO/Li[COSAN] with added LiCl is shown.

6.3.2. PEO and Li/Na[COSAN] complex in Li/Na salts

Interaction of PEO and COSAN leads to the complex formation in aqueous solution, that results in precipitation of water-insoluble complex. The salt presence influences the precipitation and stability of formed complexes. We can compare the influence of COSAN counter cation (Li^+ and Na^+) and influence of lithium and sodium salt anions. Results from this simple visual experiment (Figure 44 and Figure 45) will be used for design of stimuli-responsive gels and nanoparticles based on PEO/COSAN interaction. Visible difference was in sample with lithium sulphate right after preparation of the samples and the next day the complex was precipitated. Precipitation occurred in sample with lithium chloride after 12 days, and we were able to see a change in lithium iodine sample after 18 days. Complex started to precipitate in the presence of lithium iodine after 1 month as well. After 3 months neither lithium chloride or lithium iodine samples were fully precipitated. In lithium fluoride and lithium thiocyanate samples no visible precipitation was observed after 3 months. In comparison, all sodium salts, show visible changes already 2 days after preparation. A precipitation formed in all samples in the 3 weeks. Samples were fully precipitated with the exception of sodium sulphate sample in 3 months. Even after three months of observation PEO/COSAN complex did not fully precipitate in sodium sulphate sample. We can reliably say that the counter ion matters in the stability of the PEO/COSAN complexes. But what

also matters is the combination of the chosen cation and anion, best shown on the example of the sulfate, where in case of lithium sulfate we see precipitation the next day after preparation, but in case of sodium sulfate the sample is not completely precipitated even after three weeks.

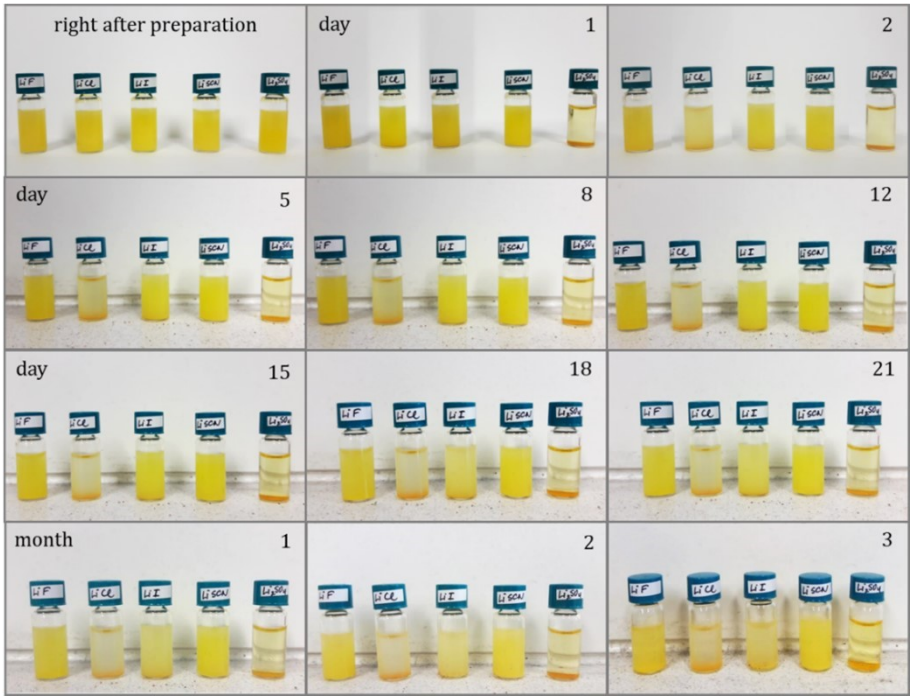

Figure 44: Samples with PEO/Li[COSAN]/Li salts systems over the course of 3 months.

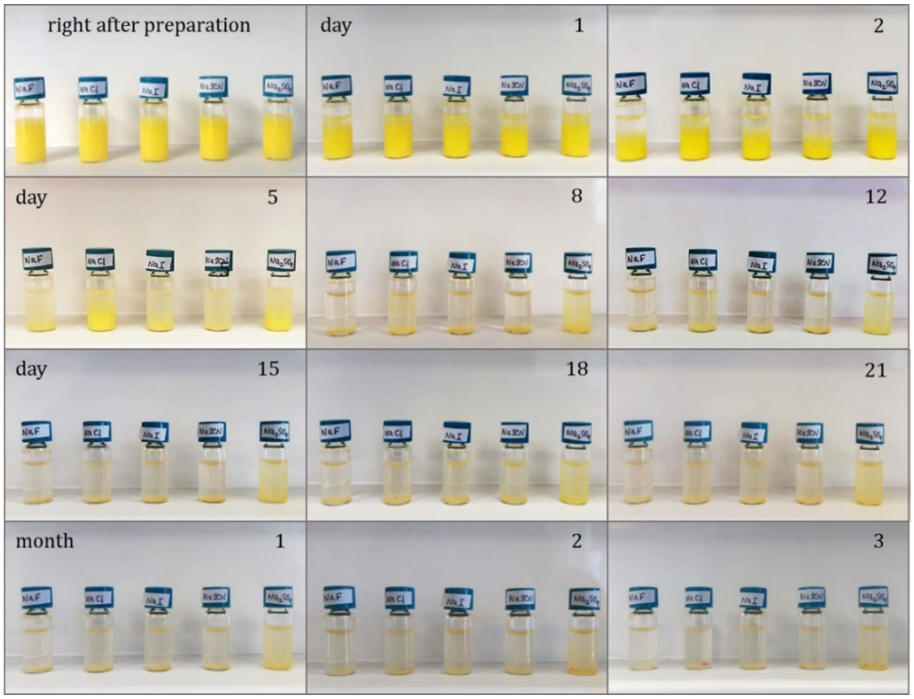

Figure 45: Samples with PEO/Na[COSAN]/Na salts systems over the course of 3 months.

7. Conclusion

By co-assembly of triblock copolymers PGEA-PEO-PGEA with *closo*-dodecaborate anion, $[B_{12}H_{12}]^{2-}$, in pure water and in 0.1 M NaCl solution, and co-assembly of triblock copolymers PNIPAM-PAA-PNIPA with cobalt bis(1,2-dicarbollite), COSAN, prepared were diverse nanomaterials spanning from gels to low-viscous solutions. Nanomaterials were characterized by variety of scattering techniques, fluorescence spectroscopy and rheology measurements. The PEO/COSAN insoluble complexes in aqueous solutions were also prepared and impact of the variety of lithium and sodium salts on the stability of PEO/COSAN in water solutions was studied.

Triblock copolymers PGEA-PEO-PGEA formed hydrogels with dodecaborate in aqueous solutions. By DLS technique, we observed transition from gels to freely moving particles by dilution of gels with water, which depends on the length of PGEA blocks. Gels with shorter PGEA block (20 units) transform from gels to liquid at higher polymers concentrations. Extensive rheology study revealed the impact of PGEA blocks and added NaCl on mechanical properties of the gels. Gels with PGEA block with 40 units form stronger gels in both pure water and salt. Furthermore, the gels exhibit self-healing properties, which can be tuned by NaCl addition.

Successful synthesis of triblock copolymers PNIPAM-PAA-PNIPAM was confirmed by NMR spectroscopy and SEC. Triblock copolymers PNIPAM-PAA-PNIPAM formed gels with COSAN in aqueous solutions. By DLS measurements at low polymer concentrations, we observed response to temperature increase, which is different for pure polymer in water and system of polymer/COSAN in water. Rheology measurements at elevated polymer concentrations show that $PNIPAM_{25}$-PAA-$PNIPAM_{25}$/COSAN forms stronger gels than $PNIPAM_{50}$-PAA-$PNIPAM_{50}$/COSAN. Both COSAN containing gels show increase of storage modulus with increasing temperature revealing their thermoresponsivity. The samples without a presence of COSAN do not provide stable gels above LCST of PNIPAM blocks.

Na[COSAN] and Li[COSAN] were prepared by cation exchange. The stability and formation of the PEO/COSAN precipitants in aqueous solutions in presence of variety of lithium and sodium salts were extensively studied. The presence of salt strongly influences

the complex stability and the rate of its precipitation depending on both cation and anion of the added salt.

8. References

1. Moad, G., Rizzardo, E. and Thang, S.H., *RAFT Polymerization and Some of its Applications,* Chem. Asian J., **2013**, 8: 1634-1644. DOI: 10.1002/asia.201300262.
2. Destarac, M., *On the Critical Role of RAFT Agent Design in Reversible Addition-Fragmentation Chain Transfer (RAFT) Polymerization,* Polym. Rev, **2011**, 51, 163–187, DOI: 10.1080/15583724.2011.568130.
3. Tian X., Ding J., Zhang B., Qiu F., Zhuang X., Chen Y., *Recent Advances in RAFT Polymerization: Novel Initiation Mechanisms and Optoelectronic Applications,* Polymers, **2018**; 10(3):318, DOI:10.3390/polym10030318.
4. Rizzardo E., Chen M., Chong B., Moad G., Skidmore M. and Thang S.H., *RAFT Polymerization: Adding to the Picture,* Macromol. Symp., **2007**, 248: 104-116, DOI: 10.1002/masy.200750211.
5. John T. L., Debby F., Ronald S., *Functional Polymers from Novel Carboxyl-Terminated Trithiocarbonates as Highly Efficient RAFT Agents*, Macromolecules **2002** 35 (18), 6754-6756, DOI: 10.1021/ma020362m.
6. Fink K., Uchman M., *Boron cluster compounds as new chemical leads for antimicrobial therapy*, Coord. Chem. Rev., **2021**, 431, 213684, DOI: 10.1016/j.ccr.2020.213684.
7. Fernandez-Alvarez R., Ďorďovič V., Uchman M., Matějíček P., *Amphiphiles without Head-and-Tail Design: Nanostructures Based on the Self-Assembly of Anionic Boron Cluster Compounds*, Langmuir, **2018**, 34 (12), 3541-3554, DOI: 10.1021/acs.langmuir.7b03306.
8. Zhao X., Yang Z., Chen H., Wang Z., Zhou X., Zhang H., *Progress in three-dimensional aromatic-like closo-dodecaborate*, Coordin. Chem. Rev., **2021**, 444, p. 214042, DOI: 10.1016/j.ccr.2021.214042.
9. Matějíček P., Zedník J., Ušelová K., Pleštil J., Fanfrlík J., Nykänen A., Ruokolainen J., Hobza P., Procházka K., *Stimuli-Responsive Nanoparticles Based on Interaction of Metallacarborane with Poly(ethylene oxidee)*, Macromolecules, **2009**, 42 (13), 4829-4837, DOI: 10.1021/ma900484y.
10. Ward, M. A., Georgiou, T. K., *Thermoresponsive Polymers for Biomedical Applications,* Polymers, **2011**, 3, 1215-1242. DOI: 10.3390/polym3031215.

11. Plamper F. A., Ruppel M., Schmalz A., Borisov O., Ballauff M., Müller A. H. E., *Tuning the Thermoresponsive Properties of Weak Polyelectrolytes: Aqueous Solutions of Star-Shaped and Linear Poly(N,N-dimethylaminoethyl Methacrylate)*, Macromolecules, **2007**, 40 (23), 8361-8366, DOI: 10.1021/ma071203b.
12. Doberenz F., Zeng K., Willems C., Zhang K., Groth T., *Thermoresponsive polymers and their biomedical application in tissue engineering – a review*, J. Mater. Chem. B, **2020**, 8 , 607-628, DOI: 10.1039/C9TB02052G.
13. Zhang Q., Weber C., Schubert U. S., Hoogenboom R., *Thermoresponsive polymers with lower critical solution temperature: from fundamental aspects and measuring techniques to recommended turbidimetry conditions*, Mater. Horiz., **2017**, 4 , 109-116, DOI: 10.1039/C7MH00016B.
14. Koltzenburg S., Maskos M., Nuyken O., *Polymer Chemistry*, Springer-Verlag Berlin Heidelberg, **2017**.
15. Kujawa P., Segui F., Shaban S., Diab C., Okada Y., Tanaka F., Winnik F. M., *Impact of End-Group Association and Main-Chain Hydration on the Thermosensitive Properties of Hydrophobically Modified Telechelic Poly(N-isopropylacrylamides) in Water*, Macromolecules, **2006**, 39 (1), 341-348, DOI: 10.1021/ma051876z.
16. Dai S., Ravi P., Tam K. C., *pH-Responsive polymers: synthesis, properties and applications*, Soft Matter, **2008**, 4, 435-449, DOI: 10.1039/B714741D.
17. Kocak G., Tuncer C., Butun V., *pH-Responsive polymers*, Polym. Chem., **2017**, 8 , 144-176, DOI: 10.1039/C6PY01872F.
18. Bazban-Shotorbani S., Hasani-Sadrabadi M. M., Karkhaneh A., Serpooshan V., Jacob K. I., Moshaverinia A., Mahmoudi M., *Revisiting structure-property relationship of pH-responsive polymers for drug delivery applications*, J. Control. Release, **2017**, 253, 46-63, DOI: 10.1016/j.jconrel.2017.02.021.
19. Swift T., Swanson L., Geoghegan M., Rimmer S., *The pH-responsive Behaviour of Poly(acrylic acid) in Aqueous Solution is Dependent on Molar Mass*, Soft Matter, **2016**, 12 , 2542 —2549, DOI: 10.1039/C5SM02693H.
20. Etika, K. C.; Cox, M. A., Grunlan, J. C., *Tailored Dispersion of Carbon Nanotubes in Water with PH-Responsive Polymers*, Polymer (Guildf), **2010**, 51, 1761-1770. DOI: 10.1016/j.polymer.2010.02.024.
21. Qiang X., Chakroun R., Janoszka N., Gröschel A. H., *Self-Assembly of Multiblock Copolymers*, Isr. J. Chem., **2019**, 59, 945, DOI: 10.1002/ijch.201900044.

22. Stuart M.A.C., Hofs B., Voets I.K., de Keizer A., *Assembly of polyelectrolyte-containing block copolymers in aqueous media*, Current Opinion in Colloid & Interface Science, **2005**, 10, 30-36, DOI: 10.1016/j.cocis.2005.04.004.
23. Sheng Y., An J., Zhu Y., *Self-assembly of ABA triblock copolymers under soft confinement*, Chem. Phys., **2015**, 452, 46-52, DOI: 10.1016/j.chemphys.2015.02.019.
24. Widin J. M., Schmitt A. K., Schmitt A. L., Im K., Mahanthappa M. K., *Unexpected Consequences of Block Polydispersity on the Self-Assembly of ABA Triblock Copolymers*, Journal of the American Chemical Society, **2012**, 134 (8), 3834-3844, DOI: 10.1021/ja210548e.
25. Riess G., *Micellization of block copolymers*, Prog. Polym. Sci., **2003**, 28 (7), 1107-1170, DOI: 10.1016/S0079-6700(03)00015-7.
26. Cölfen, H., *Double-Hydrophilic Block Copolymers: Synthesis and Application as Novel Surfactants and Crystal Growth Modifiers*, Macromol. Rapid Commun., **2001**, 22: 219-252, DOI: 10.1002/1521-3927(20010201)22:4<219::AID-MARC219>3.0.CO;2-G.
27. Sanson N., Bouyer F., Destarac M., In M., Gérardin C., *Hybrid Polyion Complex Micelles Formed from Double Hydrophilic Block Copolymers and Multivalent Metal Ions: Size Control and Nanostructure*, Langmuir, **2012**, 28 (8), 3773-3782, DOI: 10.1021/la204562t.
28. Soni K. S., Desale S. S., Bronich T. K., *Nanogels: An overview of properties, Biomedical applications and obstacles to clinical translation*, Journal of Controlled Release, **2016**, 240, 109-126, DOI: 10.1016/j.jconrel.2015.11.009.
29. Li Y., Maciel D., Rodrigues J., Shi X., Tomás H., *Biodegradable Polymer Nanogels for Drug/Nucleic Acid Delivery*, Chemical Reviews, **2015**, 115 (16), 8564-8608, DOI: 10.1021/cr500131f.
30. Hoffman A.S., *Hydrogels for biomedical applications*, Adv. Drug. Deliv. Rev., **2012**, 64, 18-23, DOI: 10.1016/j.addr.2012.09.010.
31. Ullah F., Othman M.B.H., Javed F., Ahmad Z., Akil H.M., *Classification, processing and application of hydrogels: a review*, Mater. Sci. Eng. C Mater. Biol. Appl., **2015**, 57, 414-433, DOI: 10.1016/j.msec.2015.07.053.
32. Hubbell J.A., *Synthetic biodegradable polymers for tissue engineering and drug delivery*, Curr. Opin. Solid State Mater. Sci., **1998**, 3, 246-251, DOI: 10.1016/S1359-0286(98)80098-3.

33. Besghini D., Mauri M., Simonutti R., *Time Domain NMR in Polymer Science: From the Laboratory to the Industry,* Applied Sciences, **2019**, 9(9):1801, DOI: 10.3390/app9091801.
34. Izunobi J. U., Higginbotham C. L., P*olymer Molecular Weight Analysis by 1H NMR Spectroscopy*, Journal of Chemical Education, **2011**, 88 (8), 1098-1104, DOI: 10.1021/ed100461v.
35. Hatada K., Kitayama T., *NMR Spectroscopy of Polymers,* Springer-Verlag Berlin, Heidelberg, **2004**.
36. Kleckner I.R., Foster M.P., *An introduction to NMR-based approaches for measuring protein dynamics*, Biochim. Biophys. Acta, **2011**, 1814 (8), 942-968, DOI: 10.1016/j.bbapap.2010.10.012.
37. Munk P., Aminabhavi T. M., *Introduction to macromolecular science,* 2nd ed., New York: Wiley, **2002**.
38. Minton A. P., *Recent applications of light scattering measurement in the biological and biopharmaceutical sciences,* Anal. Biochem., **2016**, May 15; 501:4-22, DOI: 10.1016/j.ab.2016.02.007.
39. Pusey P.N., Van Megen W., *Dynamic light scattering by non-ergodic media*, Phys A Stat Mech Appl, 157, **1989**, 705-741, DOI: 10.1016/0378-4371(89)90063-0.
40. Matějíček P., *Physical chemistry of macromolecules*, [lecture], Prague, Charles University, Faculty of Science, **2021.**
41. Mailer A. G. et al, *Particle sizing by dynamic light scattering: non-linear cumulant analysis*, J. Phys.: Condens. Matter, **2015**, 27, 145102, DOI: 10.1088/0953-8984/27/14/145102.
42. Antony T., Saxena A., Roy K. B., Bohidar H. B., *Laser light scattering immunoassay: An improved data analysis by CONTIN method*, J. Biochem. Biophys. Methods, **1998**, 36, 75-85, DOI: 10.1016/S0165-022X(97)00047-X.
43. Mori S., Bartj H. G., *Size Exclusion Chromatography*, Springer Science & Business Media, **1999**.
44. Hunt B. J., Holding S. R., *Size Exclusion Chromatography*, Springer Science & Business Media, **2013**.
45. Striegel A.M., *Size exclusion chromatography Liquid Chromatography: Fundamentals and Instrumentation*, 2nd ed., Elsevier, **2017**.

46. Procházka K. et al., *Fluorescence Spectroscopy as a Tool for Investigating the Self-Organized Polyelectrolyte Systems*, Adv Polym Sci, **2011**, 241: 187–249, DOI: 10.1007/12_2010_56.
47. Obšil T., *Biophysical chemistry I*, [lecture], Prague, Charles Univerity, Faculty of Science, **2021**.
48. Lakowicz J. R., *Principles of fluorescence spectroscopy*, 2nd ed.; Springer: New York, **2006.**
49. Albani J. R., *Principles and applications of fluorescence spectroscopy*, Blackwell Science: Oxford, **2007**.
50. Smith T. A. Ghiggino K. P., *A review of the analysis of complex time-resolved fluorescence anisotropy data*, Methods Appl. Fluoresc., **2015,** 3 022001, DOI: 10.1088/2050-6120/3/2/022001.
51. Strachota A., *Polymer physics and rheology*, [lecture], Prague, Charles University, Faculty of Science, **2021.**
52. Goodwin J. W., Hughes R. W., Rheology for Chemists: An Introduction, 2nd ed., Royal Society of Chemistry, **2008**.
53. Shaw M. T., *Introduction to Polymer Rheology*, John Wiley & Sons, **2012**.
54. Böhme G., *Non-Newtonian Fluid Mechanics*, Elsevier, **2012**.
55. Ingham B., *X-ray scattering characterisation of nanoparticles*, Crystallography Reviews, **2015**, 21:4, 229-303, DOI: 10.1080/0889311X.2015.1024114.
56. Li T., Senesi A. J., Lee B., *Small Angle X-ray Scattering for Nanoparticle Research*, Chemical Reviews, **2016**, 116 (18), 11128-11180, DOI: 10.1021/acs.chemrev.5b00690.
57. Ares A.E., *X-ray Scattering*, BoD-Books on Demand, **2017**.
58. Li J., Janoušková O., Fernandez-Alvarez R., Mesíková S., Tošner Z., Kereïche S., Uchman M., Matějíček P., *Designed Boron-Rich Polymeric Nanoparticles Based on Nano-ion Pairing for Boron Delivery*, Chem. Eur. J., **2020**, 26, 14283, DOI: 10.1002/chem.202001699.
59. Matějíček P., Brus J., Jigounov A., Pleštil J., Uchman M., Procházka K., Gradzielski M., *On the Structure of Polymeric Composite of Metallacarborane with Poly(ethylene oxide)*, Macromolecules 44 (10), **2011**, 3847-3855, DOI: 10.1021/ma200502t.